FAULT TOLERANT CONTROL ALLOCATION IN SYSTEMS WITH FIXED MAGNITUDE DISCRETE CONTROLS

A Thesis

by

MONIKA MARWAHA

Submitted to the Office of Graduate Studies of
Texas A&M University
in partial fulfillment of the requirements for the degree of

MASTER OF SCIENCE

December 2008

Major Subject: Aerospace Engineering

FAULT TOLERANT CONTROL ALLOCATION IN SYSTEMS WITH FIXED MAGNITUDE DISCRETE CONTROLS

A Thesis

by

MONIKA MARWAHA

Submitted to the Office of Graduate Studies of
Texas A&M University
in partial fulfillment of the requirements for the degree of

MASTER OF SCIENCE

Approved by:

Chair of Committee,	John Valasek
Committee Members,	S. R. Vadali
	A. Datta
Head of Department,	Helen Reed

December 2008

Major Subject: Aerospace Engineering

ABSTRACT

Fault Tolerant Control Allocation in Systems with Fixed Magnitude Discrete Controls. (December 2008)

Monika Marwaha, B.E., Punjab Engineering College, Chandigarh, India

Chair of Advisory Committee: Dr. John Valasek

The promise and potential of controllers that can reconfigure themselves in the case of control effector failures and uncertainties, and yet guarantee stability and provide satisfactory performance, has led to fault tolerant control being an active area of research. This thesis addresses this issue with the design of two fault tolerant nonlinear Structured Adaptive Model Inversion control schemes for systems with fixed magnitude discrete controls. Both methods can be used for proportional as well as discrete controls. However, discrete controls constitute a different class of problems than proportional controls as they can take only binary values, unlike proportional controls which can take many values.

Two nonlinear control laws based on Structured Adaptive Model Inversion are developed to tackle the problem of control failure in the presence of plant and operating environment uncertainties. For the case of redundant actuators, these control laws can provide a unique solution. Stability proofs for both methods are derived and are presented in this thesis.

Fault Tolerant Structured Adaptive Model Inversion that has already been developed for proportional controls is extended here to discrete controls using pulse width modulation. A second approach developed in this thesis is Fault Tolerant Control Allocation. Discrete control allocation coupled with adaptive control has not been addressed in the literature to date, so Fault Tolerant Control Allocation for discrete controls is integrated with SAMI to produce a system which not only handles discrete

control failures, but also accounts for uncertainties in the plant and in the operating environment.

Fault tolerant performance of both controllers is evaluated with non real-time nonlinear simulation for a complete Mars entry trajectory tracking scenario, using various combinations of control effector failures. If a fault is detected in the control effectors, the fault tolerant control schemes reconfigure the controls and minimize the impact of control failures or damage on trajectory tracking. The controller tracks the desired trajectory from entry interface to parachute deployment, and has an adaptation mechanism that reduces tracking errors in the presence of uncertainties in environment properties such as atmospheric density, and in vehicle properties such as aerodynamic coefficients and inertia. Results presented in the thesis demonstrate that both control schemes are capable of tracking pre-defined trajectories in the presence of control failures, and uncertainties in system and operating environment parameters, but with different levels of control effort.

To dearest Mom for her love and sacrifice

ACKNOWLEDGMENTS

I am most grateful to my thesis supervisor Dr. John Valasek for being so much more than a graduate advisor. His consistent involvement in the work and enthusiasm for discussion had always been a motivation for me. His timely advice had always been productive and enriched my understanding of the subject.

I am also indebted to Dr. Vadali and Dr. Datta for their valuable contributions to my research and for taking the time to serve on the thesis defense committee. All of my committee members have been great examples of what I can achieve with hard work and dedication. I would also like to thank Dr. David B. Doman and Dr. Michael A. Bolender of the Air Force Research Laboratory for their insightful comments and suggestions on this work. I would also thank Dr. Maruthi for his valuable comments which helped to improve this work.

A special thanks to Mrs. Knabe Karen for all the administrative help rendered during my stay at Texas A&M. I extend my thanks to the entire administrative staff of the department of aerospace engineering which ensured my smooth stay at Texas A&M.

I am thankful to my lab mates Adam, Jimmy, Amanda, James, Kenton and Carolina for helping me during my research work as well as for keeping up the jovial environment in the lab. I am also thankful to my friends Avinash, Baljeet, Pariskhit and Mrinal who helped me in many ways and made my stay at College Station so much at home.

Family is always the last to be thanked - and it is solely because their love and understanding is so dearly cherished that it feels appropriate to mention them at a point where it impresses the mind of the reader.

TABLE OF CONTENTS

CHAPTER Page

LIST OF TABLES

LIST OF FIGURES

FIGURE Page

FIGURE Page

FIGURE Page

NOMENCLATURE

Variable	Definition
C_d	Design Matrix
c_D	Coefficient of Drag
c_L	Coefficient of Lift
c_{l_β}	Rolling Moment Stability Derivative
c_{m_α}	Pitching Moment Stability Derivative
c_{n_β}	Yawing Moment Stability Derivative
D	Drag Vector
$\mathbf{g}$	Mars Gravity
h	Altitude
I	Inertia Matrix
K_d	Design Matrix
K_i	Design Matrix
L	Lift Vector
l_{ref}	Reference Length
$\mathcal{L}$	Rolling Moment
M_{aero}	Aerodynamic Moments
$\mathcal{M}$	Pitching Moment
$\mathcal{N}$	Yawing Moment
P	Positive definite matrix
$\bar{q}$	Dynamic Pressure
S_{ref}	Reference Area
T	Torque produced by jets
u_k	Binary number

Variable	Definition
u	Control Input Vector
u_s	Slack variable
V	Lyapunov Function
v	Velocity Vector
$Y_a(\boldsymbol{\sigma},\dot{\boldsymbol{\sigma}},\ddot{\boldsymbol{\sigma}})$	Regression matrix
ρ	Density of Mars atmosphere
σ	Modified Rodrigues Parameter Vector
α	Angle-of-Attack
β	Sideslip angle
γ	Flight Path Angle
ϕ	Bank Angle
ω	Angular Velocity
Γ	Learning Rate
τ_{i_des}	Desired moment
α_1	K_∞ function
α_2	K_∞ function
α_3	K_∞ function
ρ_1	K_∞ function
κ	K_∞ function
θ	Constant Inertia parameter vector
ϵ	Tracking error
δP	Error in angular velocity in Roll axis
δQ	Error in angular velocity in Roll axis
δR	Error in angular velocity in Roll axis

CHAPTER I

INTRODUCTION

To achieve the trajectory tracking accuracy requirements in case of control failures and uncertainties in plant and environment parameters, it is imperative to develop and implement sophisticated guidance and control algorithms that can sustain the effects of control failure. One of the challenges with the design of a guidance law or a controller is handling uncertainties that the system will encounter in operation. Uncertainty is defined as a difference between the real system and the mathematical model. Uncertainty can be present not only in the plant parameters, but also in the operating environment as sometimes the environment is poorly known. Adaptive control and guidance are one of the options available to the engineer to handle plant and exogenous inputs.

Another challenge during operation is recovery or tolerance in the case of control failures or faults. Control faults can be due to any malfunction in the physical system or subsystem of the controller which results in its failure to perform as designed. The main reasons for faults in controllers are

- Suspension of the control signal
- Damage or malfunction of system or subsystem of control system
- Partial or full damage to control effectors

The timely action taken by a reconfigurable controller reduces the chances of disastrous consequences. Once failure occurs, its detection and correction is important

---

The journal model is *IEEE Transactions on Automatic Control.*

to avoid any catastrophic consequences. In Reference [1] a survey of various reconfigurable control methodologies is presented and it is shown that most traditional reconfiguration control approaches rely on fault detection and isolation. The complexity of such a system with this feature grows with the increase in the number of failures, and there tends to be a significant possibility of false alarms.

There are two types of fault tolerant design methods: active and passive. In passive methods a controller is designed to handle pre-defined worst case failures. They are also called reliable methods. In active methods, also called reconfigurable methods, a control law is designed to handle every case of control failure. The control reconfigures itself if any failure occurs during operation. Therefore, to follow a reference trajectory, a fault tolerant adaptive controller is required which can adapt itself if any control failure occurs during operation. Redundant actuators are provided to handle the control failures. When the number of actuators is more than necessary to generate pitch, roll and yaw moments, multiple combinations can be found to generate these moments using these actuators. The benefit offered by having multiple solutions can be used to provide redundancy in case of failures or damage. Redundant actuation combined with a control allocation [2] algorithm can be used to provide consistent and unique solutions to the problem.

The proposed research seeks to develop an active control allocation based fault tolerant control law for systems with fixed magnitude discrete controls. Development of two fault tolerant controllers is proposed. The difference between the two controllers lies in their fault tolerant scheme. In the first scheme Fault Tolerant SAMI [3] is used to achieve the fault tolerance. Continuous control signals are converted to discrete signals using pulse width modulation. A fault detection algorithm is not required for this controller, unlike the second controller. If any control fails, Fault Tolerant SAMI reconfigures the controls, and minimizes the error between the ref-

erence trajectory and states of the plant, which occurs due to control failure. In the second approach control allocation is used to reconfigure the control laws if any fault occurs during operation. The control allocation acts as a non-uniform quantizer which generates the applied moments that approximate the desired moments generated by a continuous adaptive control law. Adaptive control is used to compute desired moments for this controller, and the commanded body rates form the input to the Structured Adaptive Model Inversion control (SAMI) [4, 5, 6, 3]. This nonlinear control law generates the commanded moments for the control allocation module which generates the optimal controls to follow the desired trajectory. If a fault is detected in the controls, it reconfigures the controls to minimize the impact of control failures or damage.

The approach developed here is demonstrated with numerical simulation results using the Mars Ellipsled vehicle of Reference [7]. The Mars Ellipsled, shown in Figure 1, requires precision trajectory tracking so that a family of vehicles can be sent to the same location on the surface.

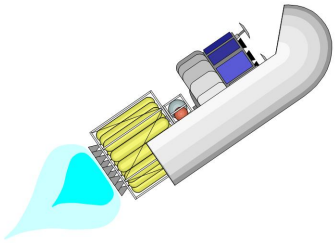

Fig. 1. Mars Ellipsled

It is critical that all Ellipsleds can land in close proximity to each other since the crew will be working with equipments and science experiments from multiple vehicles. To be able to achieve this level of landing accuracy in case of control failures and uncertainties, a controlled entry is necessary. The Ellipsled has only pulsed reaction

control jets as controllers. These controllers act as discrete devices and involve a complex on/off mechanism for operation. The mechanical devices used in the on/off mechanism of RCS jets are susceptible to failures over time, so ideally the control algorithm should be able to handle these failures.

The proposed research is unique because

1. Integration of the SAMI and control allocation algorithms in the proposed Fault Tolerant Control Allocation scheme for the discrete control jets is novel. This combination will not only handle the plant and environment uncertainties but also provide satisfactory performance in case of control failure. The stability proof for the fault tolerant controller is included.

2. The first control scheme is developed for the fixed magnitude discrete controls for the first time. The proposed scheme makes use of the fault tolerant control scheme which has already been tested for proportional controls. The existing scheme for proportional controls is modified so that it can be used for discrete controls.

3. Mars Ellipsled is the best choice to test both the algorithms. Not only does it has redundant RCS jets to test the allocation schemes and fault tolerant methods, its weight and aerodynamic data have uncertainty which requires a control scheme robust enough to handle these uncertainties along with an uncertain environment of Mars. A fault tolerant scheme has not been developed for Mars entry vehicles in the past. Also no control allocation scheme has been used which accounts for redundant discrete controls in this vehicle.

This thesis is organized as follows. Initially, the formulation of the controllers is detailed in Chapters II and III. The modeling and simulation of the Mars Ellipsled

and control equations used in this research is explained in the next chapter. Subsequently, Chapter V describes the evaluation of the controller's performance. Finally, conclusions and recommendations are presented.

CHAPTER II

FAULT TOLERANT SAMI

A. Fault Tolerant Structured Adaptive Model Inversion

Structured Adaptive Model Inversion Control (SAMI) is one of the forms which has been successfully applied to various spacecraft problems [8]. SAMI is based on the concepts of Feedback Linearization, Dynamic Inversion, and Structured Model Reference Adaptive Control. Because dynamic inversion assumes perfect knowledge of all the system parameters which are used to solve for the control, it is approximate in actual implementation due to inaccurate modeling of system parameters, in SAMI an adaptive controller is wrapped around the dynamic inversion to handle the uncertainties in system parameters. Tandale and Valasek extended this theory and developed Fault Tolerant Structured Adaptive Model Inversion control in [3] where they have successfully applied this controller to an aircraft problem using proportional controls. The Fault Tolerant Structured Adaptive Model Inversion (FSAMI) for fixed magnitude discrete control effectors is derived by extending the earlier version for continuous control effectors. Pulse width modulation (PWM) [9] is used to convert continuous signals into discrete signals, thereby approximating the continuous signals by pulses of different width. This algorithm does not depend on fault detection information and reconfigures itself if any fault occurs. The mathematical model used for handling the failure is given by the following equation

$$M_{applied} = DM_{calculated} + E \tag{2.1}$$

where D is a constant matrix and E is a constant vector.

$$\begin{bmatrix} u_{a1} \\ u_{a2} \\ u_{a3} \end{bmatrix} = \begin{bmatrix} D_{11} & 0 & 0 \\ 0 & D_{22} & 0 \\ 0 & 0 & D_{33} \end{bmatrix} \cdot \begin{bmatrix} u_{c1} \\ u_{c2} \\ u_{c3} \end{bmatrix} + \begin{bmatrix} E_1 \\ E_2 \\ E_3 \end{bmatrix} \tag{2.2}$$

In the absence of any failure, entries in the D matrix should be identity matrix and therefore the E vector should be zero. If there is any control failure, corresponding elements in the D matrix will go to zero and the E vector will go to the constant value at which the control is frozen.

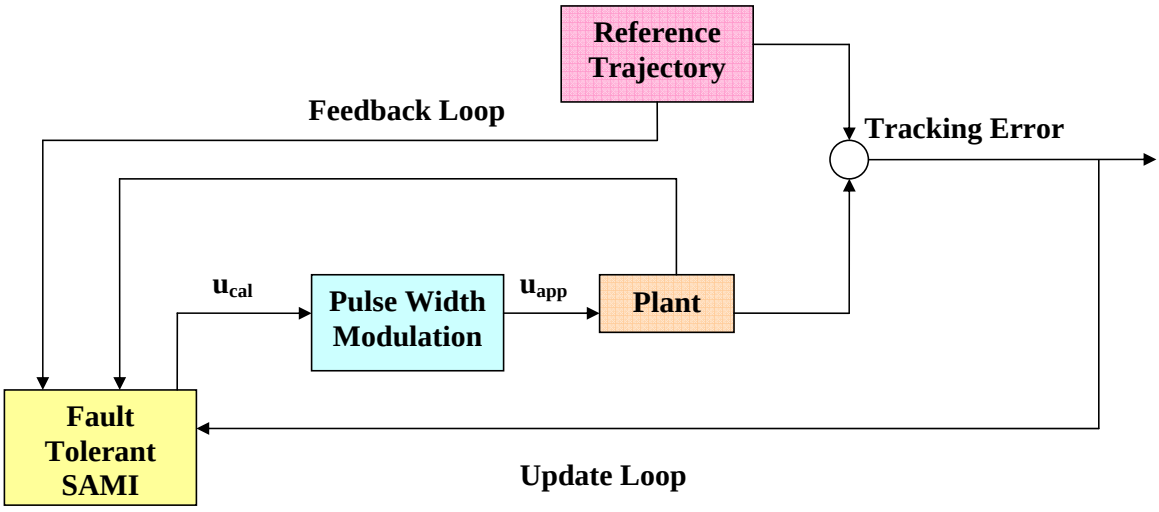

Fig. 2. Schematic of the Fault Tolerant SAMI

Figure 2 shows the schematic of the system. The tracking error feeds into the Fault Tolerant SAMI block, which updates the control based on dynamic inversion. The calculated control (u_{cal}) then becomes the input to the PWM block, which approximates the continuous signal as discrete pulses. The discrete signal (u_{app}) is then

fed into the plant. The vehicle trajectory is represented as

$$\dot{\sigma} = J(\sigma)\omega \tag{2.3}$$

$$\begin{aligned} I\dot{\omega} + \omega \times I\omega &= M_{aerodynamic} + M_{applied} \\ \dot{\omega} &= I^{-1}[M_{aerodynamic} - \omega \times I\omega] + I^{-1}M_{applied} \\ \dot{\omega} &= A(\sigma,\omega) + B(\sigma,\omega)M_{applied} \end{aligned} \tag{2.4}$$

where

$$J(\sigma) = 0.25[1 - \sigma^T\sigma]I_{3\times 3} + 2[\tilde{\sigma}] + 2\sigma\sigma^T$$

and $M_{aerodynamic}$ represents aerodynamic moments, σ are Modified Rodrigues Parameters (MRP), and ω represents angular velocity. $A(\sigma,\omega)$ represents the unforced behavior of the system and $B(\sigma,\omega)$ represents the control distribution matrix of the system. A reference model with the same states and same structure is selected to be

$$\dot{\sigma}_r = J(\sigma_r)\omega_r \tag{2.5}$$

$$\dot{\omega}_r = A(\sigma_r,\omega_r) + B(\sigma_r,\omega_r)u_r \tag{2.6}$$

Consider that the $A(\sigma,\omega)$ and $B(\sigma,\omega)$ matrices in the original plant contain uncertainties. The errors between the states and reference states can be defined as

$$s = \sigma - \sigma_r \tag{2.7}$$

$$x = \omega - \omega_r \tag{2.8}$$

$$\begin{aligned} \dot{x} &= \dot{\omega} - \dot{\omega}_r \\ \dot{x} &= A(\sigma,\omega) + B(\sigma,\omega)M_{applied} - \dot{\omega}_r \end{aligned} \tag{2.9}$$

Upon substituting the expression for $M_{applied}$ from Equation 2.1 into Equation 2.9,

the following equation for propagation of the states is obtained:

$$\dot{x} = A(\sigma, \omega) + B(\sigma, \omega)DM_{calculated} + B(\sigma, \omega)E - \dot{\omega_r} \tag{2.10}$$

The objective is to drive the error between the reference and the plant to zero, hence the following dynamics are prescribed for the error x:

$$\dot{x} = A_h x + \phi \tag{2.11}$$

where A_h is a Hurwitz matrix. All eigenvalues of this matrix lie in the left half plane so that the velocity error goes to zero asymptotically. While the choice of A_h is arbitrary, proper selection of eigenvalues permits specifying the speed at which the angular velocity error is driven to zero. Here ϕ is a forcing function on the velocity error dynamics, which helps in achieving the tracking objective. Adding and subtracting Equation 2.11 to Equation 2.10 results in

$$\dot{x} = A_h x + \phi + A(\sigma, \omega) + B(\sigma, \omega)DM_{calculated} + B(\sigma, \omega)E - (\dot{w_r} + A_h x + \phi) \tag{2.12}$$

It is assumed here that all state variables are measurable. Because the rightmost term in Equation 2.12 is known, for convenience, define this collection of variables as

$$\psi = \dot{w_r} + A_h x + \phi \tag{2.13}$$

Since system matrices A and B are uncertain and not known exactly, best guesses A_{est} and B_{est} will be used for these matrices respectively. These can be expressed as

$$C_a^* A_{est} = A \tag{2.14}$$

$$B_{est} D^* = BD \tag{2.15}$$

$$B_{est} E^* = BE \tag{2.16}$$

C_a^* is the ideal value of learning matrix C_a. Then Equation 2.12 can be written as

$$\dot{x} = A_h x + \phi + C_a^* A_{est}(\sigma, \omega) + B_{est}(\sigma, \omega) D^* M_{calculated} + B_{est}(\sigma, \omega) E^* - \psi \quad (2.17)$$

Matrices C_a^*, D^* and E^* are unknown and hence the adapted learning matrix C_a will be updated on line to ensure stability and performance of the system. C_a will account for uncertainty in the A matrix. Similarly the D matrix will account for uncertainties in the B matrix. Using dynamic inversion, we can solve for the control vector so that the velocity error x has the desired dynamics.

$$M_{calculated} = (B_{est} D)^{-1} (\psi - C_a A_{est} - B_{est} E) \quad (2.18)$$

Also using Equation 2.18, ψ can be written as

$$\psi = B_{est} D M_{calculated} + C_a A_{est} + B_{est} E \quad (2.19)$$

Equation 2.17 is updated using the value of ψ

$$\begin{aligned} \dot{x} &= A_h x + \phi + C_a^* A_{est} + B_{est} D^* M_{calculated} + & (2.20) \\ & B_{est} E^* - C_a A_{est} - B_{est} D M_{calculated} - B_{est} E & (2.21) \end{aligned}$$

$$\dot{x} = A_h x + \phi + \tilde{C}_a A_{est} + B_{est} \tilde{D} M_{calculated} + B_{est} \tilde{E} \quad (2.22)$$

where

$$\begin{aligned} \tilde{C}_a &= C_a^* - C_a & (2.23) \\ \tilde{D} &= D^* - D & (2.24) \\ \tilde{E} &= E^* - E & (2.25) \end{aligned}$$

1. Update Laws

Now let the tracking error, which includes the error terms of both the kinematic and dynamic states, be defined as

$$\begin{aligned} y &= \dot{s} + \lambda s \\ &= \dot{\sigma} - \dot{\sigma}_r + \lambda s \\ &= J\omega - J_r\omega_r + \lambda s \end{aligned} \tag{2.26}$$

where λ is a positive definite matrix. By adding and subtracting $J\omega_r$ on the RHS of Equation 2.26 it can be re-written as

$$\begin{aligned} y &= J(\omega - \omega_r) + J\omega_r - J_r\omega_r + \lambda s \\ &= Jx + J\omega_r - J_r\omega_r + \lambda s \end{aligned} \tag{2.27}$$

The following error dynamics are selected to ensure that the error converges to zero.

$$\dot{y} = A_h y \tag{2.28}$$

Now $\dot{y}$ can be calculated by differentiating Equation 2.27 with respect to time.

$$\begin{aligned} \dot{y} &= J\dot{x} + \dot{J}x + (\dot{J} - \dot{J}_r)\omega_r + (J - J_r)\dot{\omega_r} + \lambda\dot{s} \\ &= J(A_h x + \phi + \tilde{C}_a A_{est} + B_{est}\tilde{D}M_{calculated} + B_{est}\tilde{E}) \\ &\quad + \dot{J}x + (\dot{J} - \dot{J}_r)\omega_r + (J - J_r)\dot{\omega_r} + \lambda\dot{s} \end{aligned} \tag{2.29}$$

Using Equation 2.28 an expression for ϕ can be extracted. Let the sum of all known terms in Equation 2.29 be equal to the RHS of Equation 2.28.

$$JA_h x + J\phi + \dot{J}x + (\dot{J} - \dot{J}_r)\omega_r + (J - J_r)\dot{\omega_r} + \lambda\dot{s} = A_h y \tag{2.30}$$

$$\phi = J^{-1}(A_h y - \dot{J}\omega + \dot{J}_r\omega_r + J_r\dot{\omega_r} - \lambda\dot{s}) - \dot{\omega_r} - A_h x \tag{2.31}$$

Substitution of Equation 2.31 into Equation 2.29 results in

$$\dot{y} = A_h y + J(\tilde{C}_a A_{est} + B_{est}\tilde{D}M_{calculated} + B_{est}\tilde{E}) \tag{2.32}$$

To find the update laws for matrices C, D and E, the following candidate Lyapunov funtion is selected.

$$V = y^T P y + Tr(\tilde{C}_a^T W_1 \tilde{C}_a + \tilde{D}^T W_2 \tilde{D}) + \tilde{E}^T W_3 \tilde{E} \tag{2.33}$$

where P, W_1, W_2 and W_3 are positive definite matrices. Here y represents the error between position level and velocity level states, $\tilde{C}$, $\tilde{D}$ and $\tilde{E}$ represent the errors between the true and estimated matrices. Taking the time derivative of V,

$$\dot{V} = \dot{y}^T P y + y^T P \dot{y} + 2Tr(\tilde{C}_a^T W_1 \dot{\tilde{C}}_a + \tilde{D}^T W_2 \dot{\tilde{D}}) + 2\tilde{E}^T W_3 \dot{\tilde{E}} \tag{2.34}$$

$$\begin{aligned} \dot{V} = {} & y^T A_h^T P y + y^T P A_h y + 2(A_{est}^T \tilde{C}^T P y + M_{calculated}^T \tilde{D}^T B_{est}^T P y \\ & + \tilde{E}^T B_{est}^T P y) + 2Tr(\tilde{C}_a^T W_1 \dot{\tilde{C}}_a + \tilde{D}^T W_2 \dot{\tilde{D}}) + 2\tilde{E}^T W_3 \dot{\tilde{E}} \end{aligned} \tag{2.35}$$

Now let Q be a positive definite matrix, and using the Lyapunov equation

$$P A_h + A_h^T P = -Q \tag{2.36}$$

to substitute into Equation 2.35, produces the new expression

$$\begin{aligned} \dot{V} = - {} & y^T Q y + 2(\tilde{C}_a^T P y A_{est}^T + \tilde{C}_a^T W_1 \dot{\tilde{C}}_a + \tilde{D}^T B_{est}^T P y M_{calculated}^T \\ & + \tilde{D}^T W_2 \dot{\tilde{D}}) + 2(\tilde{E}^T B_{est}^T P y + \tilde{E} W_3 \dot{\tilde{E}}) \end{aligned} \tag{2.37}$$

$$\begin{aligned} \dot{V} = {} & -y^T Q y + 2Tr(\tilde{C}_a^T P y A_{est}^T + W_1 \tilde{C}_a) + \tilde{D}^T (B_{est}^T P y M_{calculated}^T \\ & + W_2 \dot{\tilde{D}}) + \tilde{E}^T (B_{est}^T P y + W_3 \dot{\tilde{E}}) \end{aligned} \tag{2.38}$$

To make $\dot{V}$ negative definite, the following adaptive laws are selected to update these

parameters in real time.

$$\begin{aligned}\dot{C}_a &= -W_1^{-1}(J^T P y A_{est}^T) \\ \dot{D} &= -W_2^{-1}(B_{est}^T J^T P y u^T) \\ \dot{E} &= -W_3^{-1}(B_{est}^T J^T P y)\end{aligned} \tag{2.39}$$

2. Stability Analysis

Using the update laws in Equation 2.39, $\dot{V}$ takes the form

$$\dot{V} = -y^T Q y \tag{2.40}$$

The Lyapunov function is a function of $\tilde{C}, \tilde{D}, \tilde{E}$ and error y. This Lyapunov function is zero when all these terms are equal to zero. The time derivative of V is zero if $y = 0$ since it is a function of only the error y. Thus $\dot{V}$ is negative semi-definite. This shows that $\tilde{C}, \tilde{D}, \tilde{E} \in L_\infty$ and $y \in (L_2 \cap L_\infty)$. From the expression for y in Equation 2.26, it is concluded that the error $s + \lambda \dot{s} \in (L_2 \cap L_\infty)$. Reference trajectories σ_r and $\dot{\sigma_r}$ are bounded, and hence $\in L_\infty$. As s and $\dot{s} \in L_\infty$ and the reference trajectories are bounded, it is concluded from the definition of s and $\dot{s}$ that $(\sigma, \dot{\sigma}) \in L_\infty$. Using the kinematic relation between σ and ω, it is concluded that $\omega \in L_\infty$ and hence $A(\sigma, \omega)$ and $\phi \in L_\infty$. All of the terms in the expression for $\dot{y}$ are bounded, and hence $\dot{y}$ is also bounded. From the properties of V and $\dot{V}$ and using Barbalat's Lemma [10], it is concluded that $\sigma \to \sigma_r$ and $\omega \to \omega_r$ as $t \to \infty$. Hence perfect tracking can be assured for both the kinematic and dynamic level states.

B. Pulse Width Modulation

Pulse width modulation is used here to approximate the continuous commanded signal produced by SAMI with discrete pulses of varying width. Since SAMI is a continuous

control law and does not have any knowledge of the discrete nature of the control effectors, it assumes that all controls are proportional, and calculates the commanded control value for each discrete control effector. PWM can be further used to convert these continuous signals to discrete pulses. Since the discrete control effectors considered in this work produce a constant magnitude control input, only the width of the pulses, not the magnitude, can be modulated. PWM is based on the concept that the pulse width of a square wave can be modulated to obtain the average value of the continuous signal. The average value of the waveform is given by

$$\bar{y} = \frac{1}{T} \int_0^T f(t) \tag{2.41}$$

As shown in Figure 3 the value of the wave is minimum (y_{min}) during $D_c.T < t < T$

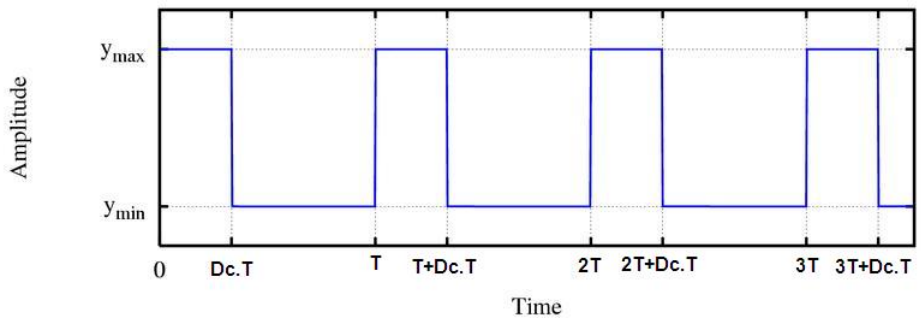

Fig. 3. Pulse Width Modulation

and maximum y_{max} during $0 < t < D_c.T$ where D_c is the duty cycle of the wave, which is defined as the time period during which the system is active. Equation 2.41

can be expanded as

$$\begin{aligned}\bar{y} &= \frac{1}{T}\left(\int_{0}^{D_cT} y_{\max}dt + \int_{D_cT}^{T} y_{\min}dt\right) \\ &= \frac{D_c.T.y_{\max} + T.(1-D_c)y_{\min}}{T} \\ &= D_c.y_{\max} + (1-D_c)y_{\min} \end{aligned} \tag{2.42}$$

If y_{min} is 0, Equation 2.42 reduces to

$$\bar{y} = D_c.y_{\max} \tag{2.43}$$

which shows the dependency of $\bar{y}$ on the duty cycle D_c.

One of the ways to calculate the duty cycle is to make it equal to the amplitude of the normalized pulse. For the case of more than one discrete control, the pulse width modulation will be different for each effector. Because of the presence of different duty cycles, the integration becomes numerically complex. Therefore to simplify numerical integration, the Euler method is used instead of more complex Runge-Kutta schemes. For the simulations, the pulse frequency is kept the same for all controls and the duty cycle differs according to the amplitude of the commanded continuous control signal. For integration all of the duty cycle time periods are sorted and then all of the small time periods are integrated in one time step. This results in an accurate integration.

CHAPTER III

FAULT TOLERANT CONTROL ALLOCATION

The second approach integrates Fault Tolerant Control Allocation for discrete controls with SAMI to produce a system which not only handles discrete control failures, but also accounts for uncertainties in the plant and in the operating environment. The adaptive control generates the desired rolling, pitching and yawing moments to follow the given trajectory. There are many ways to achieve these moments using the redundant discrete controllers. In their basic form control allocation algorithms are useful for finding solutions to meet desired control objectives by delivering the desired moments [11]. Bodson provides a comprehensive survey of constrained, numerical based optimization methods for control allocation in Reference [2], and Page and Steinberg in Reference [12] compare closed and open-loop performance for 16 different control allocation approaches. While numerous linear control allocation algorithms are currently available, Reference [13] discusses them specifically in the context of next generation entry vehicles. Application of control allocation is also shown in Reference [14]. Recently Bolender and Doman have used a concept in which control allocation is used for the aerodynamic surfaces, and dynamic inversion based adaptive control is used for system identification, which helps in identifying any failure [15]. The control variable rates or moments are nonlinear functions of control positions. These schemes are applied to different aerovehicles and are shown to have good performance for continuous controls. However, this approach has not been applied to discrete controls, since they require a different allocation algorithm than aerodynamic surfaces [16]. In this approach, the discrete control allocation algorithm of Reference [17] is used, which treats the reaction control system (RCS) control jets as quantized elements. Mixed Integer Linear Programming is used for the optimization problem. The struc-

ture of the adaptive control with discrete control allocation scheme is shown in Figure 4. The tracking error between the reference trajectory and plant states is used to update the dynamic inversion based control law. The controls (u_{cal}) calculated by the adaptive control module become the commanded control. The control signal feeds a control allocation module, and then the optimal control (u_{app}) calculated in this module become the control which is applied to the plant. The reference trajectory, plant states, and tracking error are all fed back to the dynamic inversion controller.

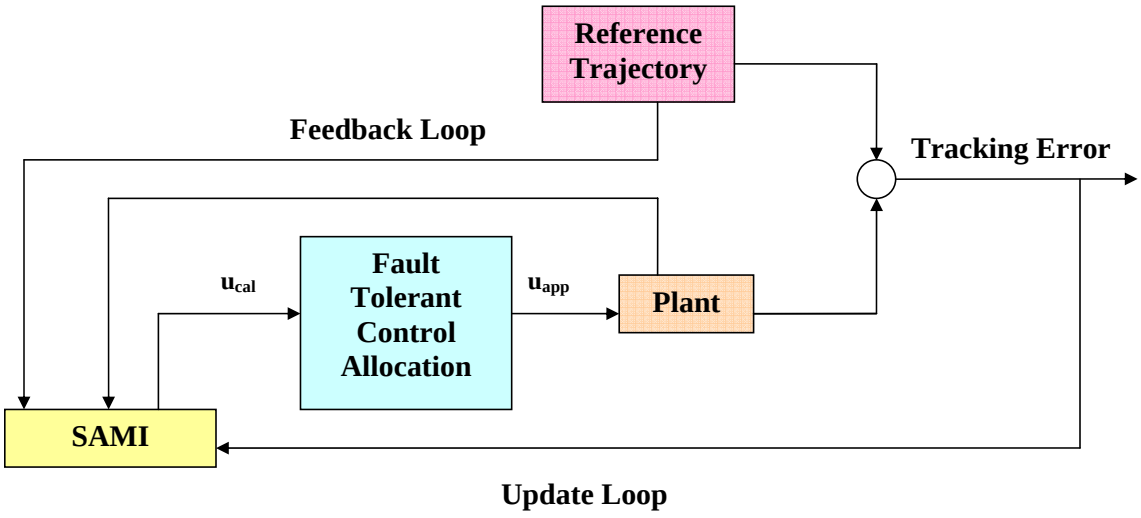

Fig. 4. Schematic of the Fault Tolerant Control Allocation

A. Structured Adaptive Model Inversion

The nonlinear plant can be modeled as

$$\dot{\sigma} = J(\sigma)\omega \tag{3.1}$$

$$\dot{\omega} = -I^{-1}(\tilde{\omega}I\omega) + I^{-1}(u + M_{aero}) \tag{3.2}$$

where

$$M_{aero} = \text{Aerodynamic Moments} = \bar{q} S_{ref} l_{ref} \begin{bmatrix} c_{l\beta}\beta \\ c_{m\alpha}\alpha \\ c_{n\beta}\beta \end{bmatrix}$$

and $\tilde{\omega}$ represents skew symmetric matrix given by

$$[\tilde{\omega}] = \begin{bmatrix} 0 & -\omega_3 & \omega_2 \\ \omega_3 & 0 & -\omega_1 \\ -\omega_3 & \omega_1 & 0 \end{bmatrix}$$

σ represents MRPs and ω represents angular velocity. $J(\sigma)$ is the nonlinear transformation relating $\dot{\sigma}$ and ω. As done in the first approach, consider a reference model having a structure similar to that of the nonlinear plant with states σ_r and ω_r. The control objective is to calculate the commanded moments which track the reference trajectory in terms of σ_r and ω_r where σ_r represent the reference MRPs and ω_r are the reference angular velocities and Equation 3.1 and Equation 3.2 can be rearranged to obtain the following form [18]

$$I_a^*(\sigma)\ddot{\sigma} + C_a^*(\sigma, \dot{\sigma})\dot{\sigma} = P_a^T(\sigma)(u + M_{aero}) \tag{3.3}$$

where

$$P_a(\sigma) = J^{-1}(\sigma)$$

$$I_a^*(\sigma) = P_a^T I P_a$$

$$C_a^*(\sigma, \dot{\sigma}) = I_a^* \dot{J}_a P_a + P_a^T [\widetilde{P_a \dot{\sigma}}] I P_a$$

Here we will consider aerodynamic moments, which are modeled by separating the known and unknown terms. In the expression for the aerodynamic moments everything is assumed to be known except for atmospheric density and the aerodynamic

coefficients of the vehicle. These uncertain terms are separated in a column denoted by d^*.

$$M_{aero} = \frac{1}{2} S_{ref} l_{ref} v^2 \begin{bmatrix} \beta & 0 & 0 \\ 0 & \alpha & 0 \\ 0 & 0 & \beta \end{bmatrix} \underbrace{\begin{bmatrix} \rho c_{l\beta} \\ \rho c_{m\alpha} \\ \rho c_{n\beta} \end{bmatrix}}_{d^*} \tag{3.4}$$

Let D_{est} be the guess for d^* and d is the gain matrix which adapts itself so that

$$d^* = D_{est} d \tag{3.5}$$

Equation 3.4 can now be written as

$$M_{aero} = \frac{1}{2} S_{ref} l_{ref} v^2 \begin{bmatrix} \beta & 0 & 0 \\ 0 & \alpha & 0 \\ 0 & 0 & \beta \end{bmatrix} D_{est} d \tag{3.6}$$

Using the minimal parametrization of inertia matrix given by

$$\begin{bmatrix} I_{11} & I_{12} & I_{13} \\ I_{12} & I_{22} & I_{23} \\ I_{13} & I_{23} & I_{33} \end{bmatrix} \begin{bmatrix} a_1 \\ a_2 \\ a_3 \end{bmatrix} = \begin{bmatrix} a_1 & 0 & 0 & a_2 & a_3 & 0 \\ 0 & a_2 & 0 & a_1 & 0 & a_3 \\ 0 & 0 & a_3 & 0 & a_1 & a_2 \end{bmatrix} \begin{bmatrix} I_{11} \\ I_{22} \\ I_{33} \\ I_{12} \\ I_{13} \\ I_{23} \end{bmatrix} \tag{3.7}$$

i.e. the product of the inertia matrix and any vector a can be written as

$$I\boldsymbol{a} = \Lambda(\boldsymbol{a})\boldsymbol{\theta}, \quad \forall \boldsymbol{a} \in \mathbb{R}^3 \tag{3.8}$$

one can linearly parametrized the the left hand side of Equation 3.3

$$I_a^*(\boldsymbol{\sigma})\ddot{\boldsymbol{\sigma}} + C_a^*(\boldsymbol{\sigma}, \dot{\boldsymbol{\sigma}})\dot{\boldsymbol{\sigma}} = Y_a(\boldsymbol{\sigma}, \dot{\boldsymbol{\sigma}}, \ddot{\boldsymbol{\sigma}})\boldsymbol{\theta} \tag{3.9}$$

where $\boldsymbol{\theta}$ is the constant inertia parameter vector defined as $\boldsymbol{\theta} \triangleq \begin{bmatrix} I_{11} & I_{22} & I_{33} & I_{12} & I_{13} & I_{23} \end{bmatrix}^T$ and $Y_a(\boldsymbol{\sigma},\dot{\boldsymbol{\sigma}},\ddot{\boldsymbol{\sigma}})$ is a regression matrix. The terms on the left hand side of Equation 3.9 can be written as

$$\begin{aligned} I_a^*\ddot{\boldsymbol{\sigma}} &= P_a^T I P_a \ddot{\boldsymbol{\sigma}} \\ &= P_a^T \Lambda(P_a\ddot{\boldsymbol{\sigma}})\boldsymbol{\theta} \qquad (3.10) \\ C_a^*\dot{\boldsymbol{\sigma}} &= -P_a^T I P_a \dot{J}_a P_a \dot{\boldsymbol{\sigma}} + P_a^T[\widetilde{P_a\dot{\boldsymbol{\sigma}}}] I P_a \dot{\boldsymbol{\sigma}} \\ &= P_a^T\{-\Lambda(P_a\dot{J}_a P_a\dot{\boldsymbol{\sigma}}) + [\widetilde{P_a\dot{\boldsymbol{\sigma}}}]\Lambda(P_a\dot{\boldsymbol{\sigma}})\}\boldsymbol{\theta} \qquad (3.11) \end{aligned}$$

Combining Equations 3.10 and 3.11 we have the linear minimal parameterization for the Inertia Matrix [18].

$$\begin{aligned} I_a^*(\boldsymbol{\sigma})\ddot{\boldsymbol{\sigma}} + C_a^*(\boldsymbol{\sigma}, \dot{\boldsymbol{\sigma}})\dot{\boldsymbol{\sigma}} &= P_a^T\{\Lambda(P_a\ddot{\boldsymbol{\sigma}}) - \Lambda(P_a\dot{J}_a P_a\dot{\boldsymbol{\sigma}}) + [\widetilde{P_a\dot{\boldsymbol{\sigma}}}]\Lambda(P_a\dot{\boldsymbol{\sigma}})\}\boldsymbol{\theta} \\ &= Y_a(\boldsymbol{\sigma}, \dot{\boldsymbol{\sigma}}, \ddot{\boldsymbol{\sigma}})\boldsymbol{\theta} \qquad (3.12) \end{aligned}$$

The tracking error is defined as

$$\varepsilon = \sigma - \sigma_r \tag{3.13}$$

Differentiating and multiplying by I_a^* on both sides

$$I_a^*\ddot{\epsilon} = I_a^*\ddot{\sigma} - I_a^*\ddot{\sigma}_r \tag{3.14}$$

Let C_d, K_d and K_i be the design matrices, adding $(C_a^* + C_d)\dot{\epsilon} + K_d\epsilon + K_i\int \epsilon dt$ to

both sides of Equation 3.14

$$I_a^*\ddot{\epsilon} + (C_d + C_a^*(\sigma,\dot{\sigma}))\dot{\epsilon} + K_d\epsilon + K_i\int \epsilon dt = (I_a^*\ddot{\sigma} + C_a^*(\sigma,\dot{\sigma})\dot{\sigma}) - (I_a^*\ddot{\sigma}_r + C_a^*(\sigma_r,\dot{\sigma_r})\dot{\sigma_r}) + C_d\dot{\epsilon} + K_d\epsilon + K_i\int \epsilon dt \tag{3.15}$$

Rearranging the equation above and using Equation 3.3, the RHS of the above equation can be written in the form

$$RHS = P_a^T(u + M_{aero}) - Y(\sigma,\dot{\sigma},\dot{\sigma_r},\ddot{\sigma_r})\theta + C_d\dot{\epsilon} + K_d\epsilon + K_i\int \epsilon dt \tag{3.16}$$

As mentioned above dynamic inversion is used to calculate the control and the control is given by the following equation.

$$u = P_a^{-T}\{Y_a(\sigma,\dot{\sigma},\dot{\sigma}_r,\ddot{\sigma}_r)\theta - C_d\dot{\epsilon} - K_d\varepsilon - K_i\int \epsilon dt\} - \underbrace{\frac{1}{2}S_{ref}l_{ref}v^2\begin{bmatrix}\beta & 0 & 0\\ 0 & \alpha & 0\\ 0 & 0 & \beta\end{bmatrix}D_{est}}_{L}\underbrace{\begin{bmatrix}d_1\\ d_2\\ d_3\end{bmatrix}}_{d} \tag{3.17}$$

1. Update Laws

The control law derived above is not implementable due to uncertainties present in θ and d. To implement this control law estimated parameters are used instead of unknown parameters for calculating the control. The control law takes the following

form

$$u = P_a^{-T}\{Y_a(\sigma,\dot{\sigma},\dot{\sigma}_r,\ddot{\sigma}_r)\hat{\theta} - C_d\dot{\epsilon} - K_d\varepsilon - K_i\int \epsilon dt\} - \underbrace{\frac{1}{2}S_{ref}l_{ref}v^2 \begin{bmatrix} \beta & 0 & 0 \\ 0 & \alpha & 0 \\ 0 & 0 & \beta \end{bmatrix} D_{est}}_{L} \underbrace{\begin{bmatrix} \hat{d}_1 \\ \hat{d}_2 \\ \hat{d}_3 \end{bmatrix}}_{\hat{d}} \tag{3.18}$$

Using the above control law, the closed-loop dynamics takes the following form

$$\begin{aligned} I_a^*\ddot{\epsilon} + (C_d + C_a^*(\sigma,\dot{\sigma}))\dot{\epsilon} + K_d\epsilon + K_i\int \epsilon dt &= -P_a^T L\hat{d} + P_a^T Ld + Y_a(\sigma,\dot{\sigma},\dot{\sigma}_r,\ddot{\sigma}_r)\tilde{\theta} \\ I_a^*\ddot{\epsilon} + (C_d + C_a^*(\sigma,\dot{\sigma}))\dot{\epsilon} + K_d\epsilon + K_i\int \epsilon dt &= -P_a^T L\tilde{d} + Y_a(\sigma,\dot{\sigma},\dot{\sigma}_r,\ddot{\sigma}_r)\tilde{\theta} \end{aligned} \tag{3.19}$$

where

$$\tilde{d} = \hat{d} - d$$

$$\tilde{\theta} = \hat{\theta} - \theta$$

Equation 3.19 can be written as

$$I_a^*\ddot{\epsilon} + (C_d + C_a^*(\sigma,\dot{\sigma}))\dot{\epsilon} + K_d\epsilon + K_i\int \epsilon dt = \Psi\tilde{\Phi} \tag{3.20}$$

where

$$\tilde{\Phi} = \begin{bmatrix} \tilde{\theta} & \tilde{d} \end{bmatrix}$$

$$\Psi = \begin{bmatrix} Y_a & -P_a^T L \end{bmatrix}$$

If vector

$$\mathrm{y} = \begin{bmatrix} \int \varepsilon \mathrm{dt} & \varepsilon & \dot{\varepsilon} \end{bmatrix}$$

and

$$A = \begin{bmatrix} 0 & I_{3\times3} & 0 \\ 0 & 0 & I_{3\times3} \\ -(I_a^*)^{-1}K_i I_{3\times3} & -(I_a^*)^{-1}K_d I_{3\times3} & -(I_a^*)^{-1}C_d I_{3\times3} \end{bmatrix}$$

the Equation 3.20 can be written as

$$\dot{y} = Ay + \Psi\tilde{\Phi} \tag{3.21}$$

To obtain the update laws for the estimated parameters, the following candidate Lyapunov function is selected

$$V = y^T P y + \frac{1}{2}\tilde{\Phi}^T\Gamma^{-1}\tilde{\Phi} \tag{3.22}$$

where P is a positive definite matrix and Γ is a gain matrix. Vector y consists of the tracking error, its derivative, and the integral of the tracking error. $\tilde{\Phi}$ consists of the errors between true and estimated inertia vector and true and estimated vector d, vector d includes uncertainties in aerodynamic coefficients and atmospheric density. Taking the time derivative of the Lyapunov function

$$\dot{V} = y^T P\dot{y} + \dot{y}Py + \dot{\tilde{\Phi}}^T\Gamma^{-1}\tilde{\Phi} \tag{3.23}$$

and substituting the expression for $\dot{y}$ into Equation 3.23 results in

$$\dot{V} = y^T(A^T P + PA)y + y^T P\Psi\tilde{\Phi} + \dot{\tilde{\Phi}}^T\Gamma^{-1}\tilde{\Phi} \tag{3.24}$$

Since A is a Hurwitz matrix, the Lyapunov stability criterion states that for any positive definite matrix Q, there exists a corresponding positive definite matrix P such that

$$PA + A^T P = -Q \tag{3.25}$$

Equation 3.24 becomes

$$\begin{aligned}\dot{V} &= -y^T Q y + y^T P \Psi \tilde{\Phi} + \dot{\tilde{\Phi}}^T \Gamma^{-1} \tilde{\Phi} \\ &= -y^T Q y + (y^T P \Psi + \dot{\tilde{\Phi}}^T \Gamma^{-1}) \tilde{\Phi} \end{aligned} \tag{3.26}$$

The update law selected for this system is

$$\dot{\tilde{\Phi}} = -\Gamma \Psi^T P y \tag{3.27}$$

2. Stability Analysis

This choice of update law can be used to show that

$$\dot{V} = -y^T Q y \leq 0 \tag{3.28}$$

Since $V > 0$ and $\dot{V} \leq 0$, all the terms which appear in the expression for V in Equation 3.22, i.e. y and $\tilde{\Phi} \in L_\infty$ and hence are bounded. This in turn proves that $\epsilon, \dot{\epsilon}$, and $\int \epsilon dt \in L_\infty$ as y is a vector consisting of all these terms. The reference trajectory is bounded, and hence σ_r, $\dot{\sigma_r}$ are bounded. Having proved that ϵ and σ_r are bounded, from the definition of tracking error given by Equation 3.13, σ is also bounded. This implies that $Y_a(\sigma, \dot{\sigma}, \dot{\sigma_r}, \ddot{\sigma_r})$ is bounded. Note that $\dot{V} = 0$ only if $y = 0$ regardless of the value of $\tilde{\Phi}$, and hence $\dot{V}$ is semi-negative definite. Using these properties of V and $\dot{V}$ and Barbalat's Lemma [10], it is concluded that $y \in L_2 \cap L_\infty$ and $\tilde{\Phi} \in L_\infty$. So we can conclude that ϵ and $\dot{\epsilon}$ goes to zero as t approaches ∞. Hence it is concluded that $\sigma \to \sigma_r$ and $\omega \to \omega_r$ as $t \to \infty$.

B. Control Allocation

In the present work control allocation is conducted as discussed in Reference [17], where Mixed Integer Linear Programming (MILP) [19, 20, 21] is used to implement

the quantization strategy. Thus the controller closes the loop using a control allocator which minimizes the difference between the commanded and the actual moments delivered. The problem of control allocation can be posed as

$$\min_{u} \sum_{i=1}^{3} |\tau_{i\_des} - \sum_{k=1}^{p} T_{i,k} u_k| + \sum_{k=1}^{p} w_k u_k \tag{3.29}$$

subject to the constraints

$$0 \leq \sum_{k=1}^{p} T_{i,k} u_k \leq \tau_{i\_des} \quad \forall \tau_{i\_des} \geq 0 \tag{3.30}$$

$$0 \geq \sum_{k=1}^{p} T_{i,k} u_k \geq \tau_{i\_des} \quad \forall \tau_{i\_des} < 0 \tag{3.31}$$

Here u_k is a binary number that can be either 0 or 1. It represents the discrete (on/off) state of the k^{th} control effector. τ_{i_des} is the desired moment in the i^{th} axis. $T_{i,k}$ is the torque produced by the k^{th} discrete control effector on the i^{th} axis, and $w_k \geq 0$ represents the penalty imposed on firing the k^{th} conrol effector. The inequality constraints given by Equations 3.30 and 3.31 are imposed to ensure that the effective torque will not exceed the magnitude of the torque commanded by the control laws. This constraint represents the quantization strategy, hence the control allocator transforms the continuous commanded torque vectors in $\Re^3$ to quantized torque vectors in $\Re^3$. These quantized torque vectors represent the optimal solution of the problem. The strategy is implemented using an MILP formulation due to the discrete control effectors. The control allocation is posed as a linear minimization problem, so that the MILP problem can be stated as

$$\min_{u,u_s} [w_1\, w_2\, \ldots w_p | w_{roll}\, w_{pitch}\, w_{yaw}] \begin{bmatrix} u \\ \\ u_s \end{bmatrix} \tag{3.32}$$

where u is a vector of binary variables and represents the state (on/off) of each control effector. $u_s \in R^3$ is the vector of slack variable which is defined by

$$u_s \triangleq \tau_{i\_des} - Tu \tag{3.33}$$

Here $\tau_{i\_des} \in R^3$ is the desired torque vector and T $\in R^{3\times p}$ is the matrix whose elements represent the torque that can be provided by each control effector. The constraints are

$$\begin{bmatrix} -u_s \\ Tu - u_s \\ -Tu - u_s \end{bmatrix} \leq \begin{bmatrix} 0 \\ \tau_{i\_des} \\ -\tau_{i\_des} \end{bmatrix} \tag{3.34}$$

and

$$0 \leq \sum_{k=1}^{p} T_{i,k} u_k \leq \tau_{i\_des} \quad \forall \tau_{i\_des} \geq 0 \tag{3.35}$$

$$0 \leq -\sum_{k=1}^{p} T_{i,k} u_k < -\tau_{i\_des} \quad \forall \tau_{i\_des} < 0 \tag{3.36}$$

1. Stability Analysis of Quantized Control

It is shown in Reference [22] that for a wide class of optimal regulators, the gain margin is infinite with respect to increase in gain and that decrease down to 0.5 can be tolerated. Author proves this for a class of systems which are closed loop asymptotically stable and on linearization the plant has eigenvalues strictly in left half of the plane. Though the system presented here is not asymptotically stable as shown in the last section, the same approach can be extended to prove the stability of the system with the quantized control. Quantized control can be treated as some fraction of the calculated control and if we prove that the system has some gain margin, we can use the same concept as in Reference [22]. Nonlinear systems with

input quantization have been proved stable in References [23, 24, 25]. Assumptions and discussion of the stability proof for this system are presented here. The nonlinear system considered is of the form

$$\dot{x} = f(x) + G(x)u \tag{3.37}$$

where $f(x)$ is the unforced dynamics and $G(x)$ is the full rank control effectiveness matrix of the system. Let us assume that there exists a feedback control law $u = k(x)$ with $k(0) = 0$ which makes the system globally asymptotically stable. It also ensures that for some class K_∞ functions $\alpha_1, \alpha_2, \alpha_3, \rho_1$ there exists a C^1 function $V : \Re^n \longrightarrow \Re$ which satisfies the inequalities

$$\alpha_1(|x|) \leq \alpha_2(|x|) \tag{3.38}$$

and

$$|x| \geq \rho_1(|e|) \quad \Rightarrow \quad \frac{\partial V}{\partial x} f(x, k(x) + e) \leq -\alpha_3(|x|) \tag{3.39}$$

for all $x, e \in \Re^n$. This implies that the perturbed closed-loop system

$$\dot{x} = f(x) + G(x)(k(x) + e) \tag{3.40}$$

is Input to State Stable (ISS) [26] with respect to the actuator disturbance input e. Assuming κ to be some class K_∞ function with the following property

$$\kappa(r) \geq \max_{|x| \leq r} |k(x)| \qquad \forall r \geq 0$$

we get

$$|k(x)| \leq |\kappa(x)| \qquad \forall x \tag{3.41}$$

If μ is defined as

$$q_\mu(z) = \mu q(\frac{z}{\mu}) \tag{3.42}$$

the closed-loop system with quantized feedback control law

$$u = q_\mu(k(x)) \tag{3.43}$$

becomes

$$\dot{x} = f(x) + G(x)(q_\mu k(x)) \tag{3.44}$$

This takes the form of Equation 3.40 if

$$e = q_\mu k(x) - k(x) \tag{3.45}$$

The behavior of the trajectories of Equation 3.44 for fixed μ is characterized by the following Lemma.

Lemma 1. *Assume that we have*

$$\alpha_1 \circ \kappa^{-1}(M\mu) > \alpha_2 \circ \rho_1(\Delta\mu) \tag{3.46}$$

Then the sets

$$R_1(\mu) := \left\{x : V(x) \leq \alpha_1 \circ \kappa^{-1}(M\mu)\right\} \tag{3.47}$$

and

$$R_2(\mu) := \{x : V(x) \leq \alpha_2 \circ \rho_1(\Delta\mu)\} \tag{3.48}$$

are invariant regions for the system of Equation 3.40. Moreover all solutions of Equation 3.40 that start in the set $R_1(\mu)$ enters the smaller set $R_2(\mu)$ in finite time, given by the formula

$$T_\mu = \frac{\alpha_1 \circ \kappa^{-1}(M\mu) - \alpha_2 \circ \rho_1(\Delta\mu)}{\alpha_3 \circ \rho_1(\Delta\mu)} \tag{3.49}$$

The unforced system

$$\dot{x} = f(x, 0) \tag{3.50}$$

is called forward complete if for every initial state $x(0)$ the solution $\xi(x(0), .)$ is defined for all $t \geq 0$.

Theorem 1. *Assume that the system in Equation 3.50 is forward complete and we have*

$$\alpha_2^{-1} \circ \alpha_1 \circ \kappa^{-1}(M\mu) > \rho_1(\Delta\mu) \quad \forall \mu > 0 \tag{3.51}$$

then there exists a hybrid quantized feedback control policy that makes the system globally asymptotically stable.

Proof. The zooming-out stage : Set the control to zero, and let $\mu(0) = 1$. Increase μ fast enough to dominate the rate of growth of $|x(t)|$. Then there will be a time $t_0 \geq 0$ such that

$$|x(t_0| \leq \rho_1(\Delta\mu(t_0)) < \alpha_2^{-1} \circ \alpha_1 \circ \kappa^{-1}(M\mu(t_0)) \tag{3.52}$$

hence $x(t_0)$ belongs to the set $R_1(\mu(t_0))$ given by Equation 3.47.

The Zooming in stage : For $t \geq t_0$ apply the control law in Equation 3.43. Let $\mu(t) = \mu(t_0)$ for $t \in [t_0, t_0 + T_{\mu(t_0)}]$, where $T_{\mu(t_0)}$ is given by Equation 3.49. Then $x(t + T_{\mu(t_0)})$ belongs to the set R_2. Using Equation 3.49 to calculate $T_{\omega(\mu(t_0))}$, where ω is the function defined by

$$\omega(r) := \frac{1}{M}\kappa \circ \alpha^{-1} \circ \alpha_2 \circ \rho_1(\Delta r), \quad r \geq 0 \tag{3.53}$$

For $t \in [t_0 + T_{\mu(t_0)}, t_0 + T_{\mu(t_0)} + T_{\omega(\mu(t_0))}]$, let

$$\mu(t) = \omega(\mu(t_0)) \tag{3.54}$$

We have $\mu(t_0 + T_{\mu(t_0)}) < \mu(t_0)$ by Equation 3.46, and $R_2(\mu(t_0)) = R_1(\mu(t_0 + T_{\mu(t_0)})$. So

we can conclude that $x(t_0 + T_{\mu(t_0)} + T_{\omega(\mu(t_0))})$ belongs to $R_2(\mu(t_0 + T_{\mu(t_0)}))$. Repeating the procedure now let $\mu(t) = \omega(\mu(t_0 + T_{\mu(t_0)}))$ for the next time interval of length given by Equation 3.49. Lyapunov stability of equilibrium $x = 0$ of the continuous dynamics follows from the adjustment policy for μ. Also the above analysis imples that $x(t) \to 0$ as $t \to \infty$. □

As seen from the above discussion that the system can be proved stable if it is asymptotically stable and is autonomous. To extend this proof it is assumed here that though the system presented in this work is changing with time but the variation is very very small and hence it is equivalent to an autonomous system.

CHAPTER IV

MODELING AND SIMULATION

This chapter describes the simulation set up used to evaluate the performance of both the controllers. The following sections describe the characteristics of the model used for the numerical example and different assumptions made for modeling of the vehicle and RCS control jets.

A. Vehicle Model

The vehicle model used to demonstrate both control law schemes and to evaluate their performance is a scaled down model of the Mars Ellipsled entry vehicle taken from Reference [7]. The Mars Ellipsled is a cylinder with diameter of 3.75 meters and length of 6.323 meters whose external physical characteristics are shown in Figure 5.

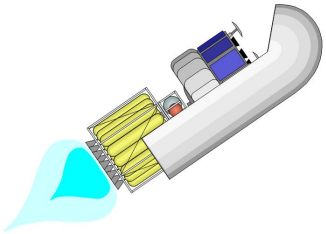

Fig. 5. Physical Charactersitics of Mars Ellipsled

The Mars Ellipsled has 18 RCS thrusters, which can be characterized as force producing devices with only two states: on and off. Each thruster is capable of producing some force $\mathbf{F} = f\hat{\mathbf{n}}$ when it is on, where f is the magnitude of thrust and $\hat{\mathbf{n}}$ is the unit vector. Therefore the torque produced by a particular thruster is calculated as $\tau = r \times f$, where r is the distance between the center of gravity and

the location of a particular thruster. There are 2^p combinations of torques that can be achieved using p number of jets. It is assumed that all of the RCS jets produce significant coupling in more than one axis (i.e roll, pitch and yaw). The time lag for the RCS jets to reach a steady-state value and conversely to ramp down to zero are not considered. Also it is assumed that the thruster performance will not decrease with time as propellant decreases. All the jets have the same efficiency, and it is constant. There are nine jets on each side, located in three clusters of three jets each: three side jets, three up jets, and three down jets. Table I provides thrust characteristics for all 18 jets.

Table I. Reaction Control System Jets

Location of Jets	Identification Numbers	Moment arm (m)	Single Jet Thrust (N)
Up Jets	1, 2, 3, 4, 5, 6	1.88	14
Side Jets	7, 8, 9, 10, 11, 12	2.98	14
Down Jets	13, 14, 15, 16, 17, 18	2.98	95

1. Equations of motion

The equations of motion are expressed in a body-fixed reference frame which is defined in Figure 6. Lift, drag and gravity forces act on the vehicle and the magnitudes of lift, drag and gravitational force are modeled using the following equations

$$L = -\bar{q}Sc_{L_\alpha}\alpha \tag{4.1}$$

$$D = -\bar{q}Sc_{D_\alpha}\alpha \tag{4.2}$$

$$F_g = mg \tag{4.3}$$

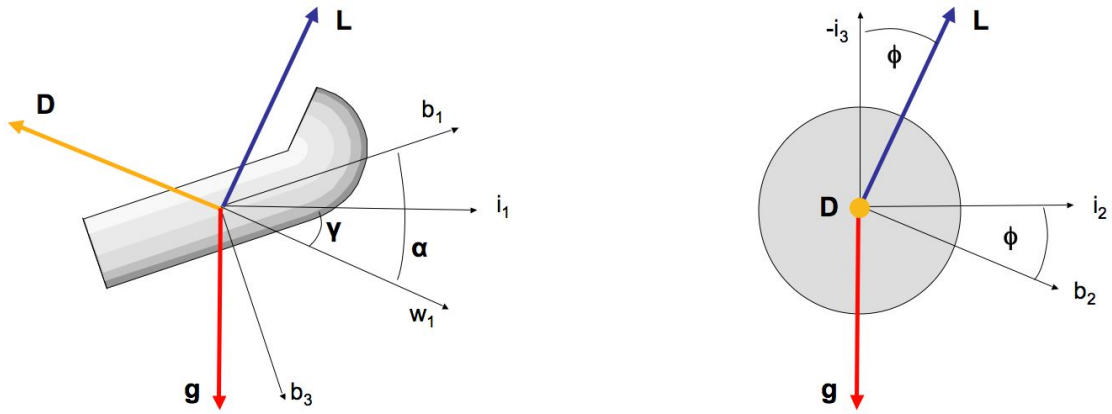

(a) Side view (b)Back view

Fig. 6. Ellipsled Free Body Diagram

From Newton's second law, the dynamic translational equations of the mass center of the vehicle are given by

$$[\mathbf{F}]_w = m\ [\mathbf{a}]_w \tag{4.4}$$

$$-D - m\ g \sin\gamma = m\dot{v} \tag{4.5}$$

$$mg\cos\gamma\sin\phi = -mv\dot{\gamma}\sin\phi \tag{4.6}$$

$$-L + mg\cos\gamma\cos\phi = -mv\dot{\gamma}\cos\phi \tag{4.7}$$

Rearranging the first equation, and adding the second and third equations, produces

$$\dot{v} = -\frac{D}{m} - g\sin\gamma \tag{4.8}$$

$$\dot{\gamma} = \frac{L}{mv}\cos\phi - \frac{g}{v}\cos\gamma \tag{4.9}$$

These equations are the translational equations of motion, or guidance equations, for the Mars Ellipsled. The rotational equations of motion for a nonlinear dynamic system that is affine in the control, can be split into a structured form consisting of an exactly known kinematic differential equation and a momentum level equation

with uncertain parameters.

$$\dot{\sigma} = J(\sigma)\omega \tag{4.10}$$

$$\dot{\omega} = A(\sigma, \omega) + B(\sigma, \omega)u \tag{4.11}$$

where $\sigma \in R^n$ is the vector of position level coordinates, and $\omega \in R^n$ is the vector of velocity level coordinates. Here the matrix J is given in terms of MRPs such that

$$J(\sigma) = 0.25[1 - \sigma^T\sigma]I_{3\times3} + 2[\tilde{\sigma}] + 2\sigma\sigma_T \tag{4.12}$$

and the A and B matrices can be developed from Equation 4.13:

$$\begin{bmatrix} \dot{\omega} \end{bmatrix} = I^{-1} \left[\begin{bmatrix} \mathcal{L} \\ \mathcal{M} \\ \mathcal{N} \end{bmatrix} - \begin{bmatrix} \tilde{\omega} I \omega \end{bmatrix} \right] + I^{-1}u \tag{4.13}$$

Here, aerodynamic moments are represented by $\mathcal{L}$, $\mathcal{M}$, and $\mathcal{N}$, and $\mathbf{u}$ is the control input from the RCS jets. The magnitudes of the aerodynamic moments are the following.

$$\mathcal{L} = \bar{q}\ S_{ref}\ l_{ref}\ c_{l_\beta}\beta \tag{4.14}$$

$$\mathcal{M} = \bar{q}\ S_{ref}\ l_{ref}\ c_{m_\alpha}\alpha \tag{4.15}$$

$$\mathcal{N} = \bar{q}\ S_{ref}\ l_{ref}\ c_{n_\beta}\beta \tag{4.16}$$

Additional details of the vehicle modeling are contained in Reference [7].

B. Reference Trajectory

The reference trajectory is given in terms of non-smooth, discrete bank angle commands as a series of step inputs. A polynomial fit is used to generate a smooth continuous command sequence which acts as an input reference trajectory to the con-

troller. The trajectory is 350 seconds long and includes several bank angle reversals as shown in Figure 7.

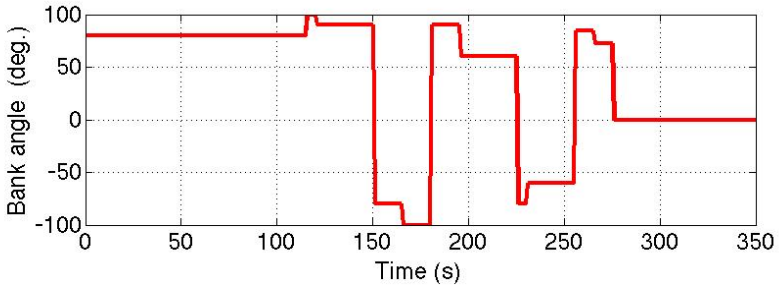

Fig. 7. Command Input Reference Trajectory

C. Numerical Examples

Two numerical examples are presented in the next chapter using both the controllers. The nonlinear, non real-time simulation model of the Mars Ellipsled is developed using the mass properties, center of gravity location, and aerodynamics given in Tables II, III, and IV respectively. There are 18 RCS jets, and the torque matrix is assumed to be constant at the values specified in the Appendix A. Since the vehicle is using 18 RCS thrusters there are 2^{18} possible combinations of thruster firing that can be used to produce the torque commanded by the reference trajectory.

The objective of the simulations is to test controller performance under plant uncertainties, with and without various combinations of control effectors. The performance of both controllers is evaluated in terms of tracking error in different states, and by the control effort used to track these states. Both the controllers cannot be compared directly due to the implementation of control schemes. Fault Tolerant SAMI generates individual commands which are calculated for each control effector, and then converts them to discrete commands using PWM. By contrast, in Fault

Tolerant Control Allocation continuous moments are calculated in three axes, and then depending upon that individual control effector the control input is calculated. For the PWM Euler integration is used to make the effect of failures less adverse. In Fault Tolerant Control Allocation a more sophisticated Runge-Kutta method is used. The specific mathematical formulations of both controllers make it difficult to inject exactly the same kind of failures in each controller, so both are evaluated separately. Each test case has uncertainties in the aerodynamic coefficients, moments of inertia, and atmospheric density. Uncertainty of 10 to 30 percent is introduced in all of the moments of inertia. The density is lumped along with the aerodynamic coefficients so that uncertainty is introduced in both of the terms together. The initial conditions for all cases are a speed of 7.3 km/sec, altitude of 125 km, and bank angle of 85 $degrees$. An initial condition error of 5 $degrees$ is introduced into the bank angle. Control failures in all cases are introduced at 2.5 seconds, and consist of a fault in the on/off firing capability of certain jets, and a corresponding decrease in their efficiency.

Table II. Ellipsled Mass and Inertia Properties

Mass	3000 kg
I_{xx}	2983 $kg \cdot m^2$
I_{yy}	4909 $kg \cdot m^2$
I_{zz}	5683 $kg \cdot m^2$

Table III. Ellipsled Geometric Properties

Reference area	S	11.045 m^2
Reference Length	l	6.323 m
x center of gravity	x_{cg}	0.182 m
y center of gravity	y_{cg}	0 m
z center of gravity	z_{cg}	-0.175 m

Table IV. Ellipsled Aerodynamics

α	c_L	c_D	c_{n_β}	$c_{m\alpha}$	c_{l_β}
45^o	0.652	1.568	-0.02	0.037	-2.279
50^o	0.659	1.740	0	0.019	-2.354
55^o	0.633	1.910	.015	0.000	-2.414
60^o	0.573	2.069	.034	-0.211	-2.462
65^o	0.481	2.208	.05	-0.428	-2.495

D. Evaluation Criteria

To evaluate the performance of both the controllers following criteria are used:

1. Is the controller robust enough to handle the control failures? Is it able to handle all types of failures?

2. How well does it perform in the presence of large initial errors in bank angle and uncertainties in plant and environment parameters?

3. What is the performance of the controller for trajectory tracking? Can it track rapidly changing trajectories? How well does it track the trajectories in the presence of control failures?

4. Does the discrete nature of the controls have any limitations for trajectory tracking or handling of control failures?

1. Test Case Definitions

The test cases evaluate different types of failures according to the criteria specified above. Results are presented first for the Fault Tolerant SAMI scheme, and then for the Fault Tolerant Control Allocation scheme. The two test cases for the Fault Tolerant SAMI controller assume that all of the jets can produce thrust in any direction, i.e. they all can produce both the positive and negative moments. This assumption is made because SAMI, being unaware of the discrete nature of the jets, produces continuous control values for each individual jet which can be either positive or negative. To apply the same moment to the system, discrete jets accommodate the magnitude of the commanded torque by varying the width of the pulses and the sign of the commanded torque by suppling both the positive and negative moments.

1. Test Case 1 = jets 2, 3, 5, 12, 15 and 17 are always on and produce a positive moment continuously throughout the trajectory. As described in Section II, Fault Tolerant SAMI generates the control values while taking into account these positive moments and reconfiguring accordingly.

2. Test Case 2 = jets 1, 2, 3, 5, 10, 12 and 15 are always on and they always produce a negative moment. Here Fault Tolerant SAMI not only calculates the control to track the reference trajectory, but also nullifies the effect of this negative moment.

Three test cases are evaluated for the Fault Tolerant Control Allocation controller. Control failures in these three cases are introduced at 2.5 seconds that consist of a fault in the on/off firing capability of certain jets and a corresponding decrease in their efficiency. The discrete control allocation scheme calculates the combinations of these controls optimally. Unlike the Fault Tolerant SAMI controller which does not require any algorithm to identify a failure, the Fault Tolerant Control Allocation controller assumes that a fault identification algorithm has already identified any failures.

1. Test Case 3 = jets 1, 2, 17 and 18 do not produce any thrust, such that the control allocation cannot use these jets.

2. Test Case 4 = jets 2 , 3, 4, 5, 8, 9 and 10 are always on. While reconfiguring the controller there is some level of thrust that is always produced by these jets.

3. Test Case 5 = some jets produce less than full thrust, e.g. if a jet can produce a thrust of 14 N it produces only 5 N due to a control malfunction in the valves or due to leakage, etc.

CHAPTER V

RESULTS

The results for both the control schemes are presented in this chapter. These results are based on the simulations performed for the cases that were discussed in the previous chapter. The results for the Fault Tolerant SAMI are presented and discussed first followed by the same for Fault Tolerant Control Allocation. The performance of the controllers is judged based on the criteria discussed in the last chapter.

A. Results for Fault Tolerant Structure Adaptive Model Inversion Controller

1. Test Case 1

Figure 8 shows a time history of the operation of the 18 RCS jets without any failure, for period of 0.1 seconds for the sake of clarity. The time history for some of the jets overlap since they stop at the same time. Therefore out of the 18 jets, the time histories of only 15 of them are visible in the figure. Note that some of the jets are marked in the figure to illustrate that the identification numbers of the jets do not necessarily correspond to the order in which they stop. In Test Case 1 jets 2, 3, 5, 7, 10, 12, 14, 15 and 17 are always on and they continuously produce a positive moment after 2.5 seconds. All of the jets operate after every 0.01 seconds. Figures 9 and 10 show that jets, which are failed after 2.5 *seconds*, are always on and rest of the jets act as pulses and try to approximate the continuous control. Time histories of all the jets are shown for only 0.01 seconds so as to illustrate their operation to the reader.

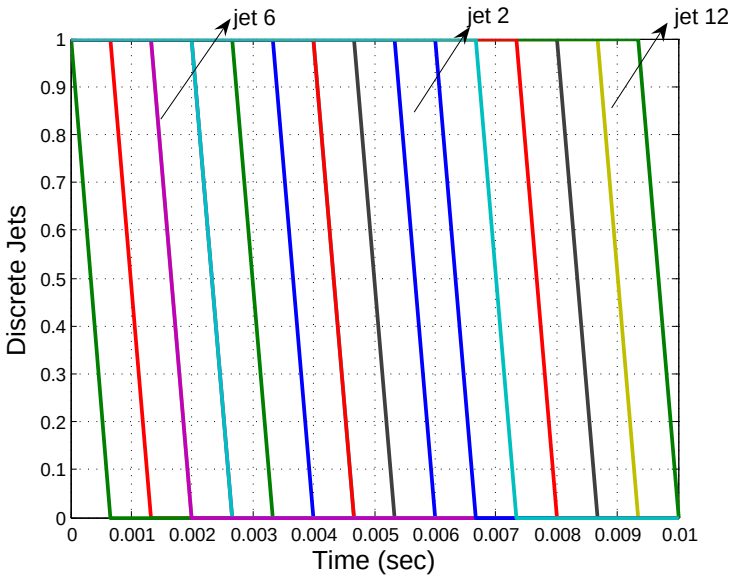

Fig. 8. Example Time History of RCS Jets

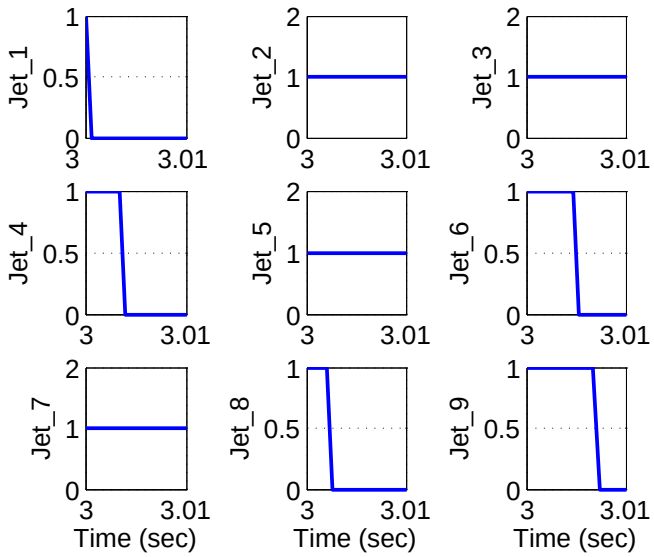

Fig. 9. Test Case 1, RCS Jets (1-9)

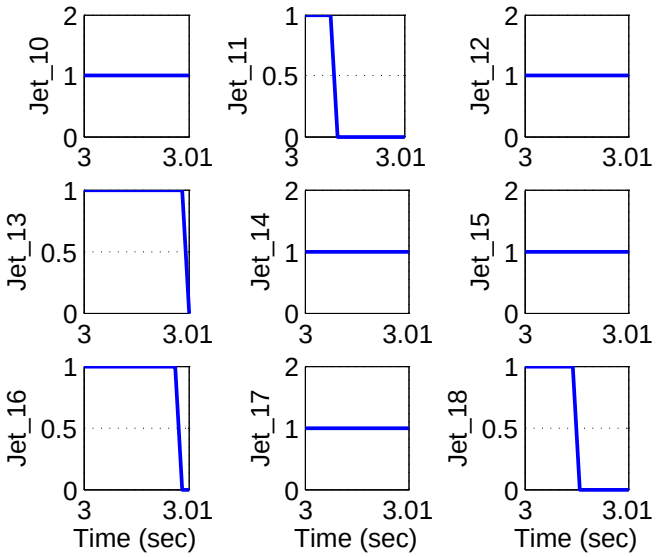

Fig. 10. Test Case 1, RCS Jets (10-18)

Figure 11 shows the bank angle trajectory. It is evident from Figure 11 that error in bank angle increases on introducing jet failure but the controller is designed such that it can reduce the error to zero and track the reference trajectory. The controller performs very well and the error quickly reduces to zero and the system tracks the reference bank angle trajectory. The effect of failure introduction is shown in Figure 12. It can be seen in this figure that as soon as the failure is introduced bank angle trajectory changes and controller reconfigures itself to bring it back to the nominal path.

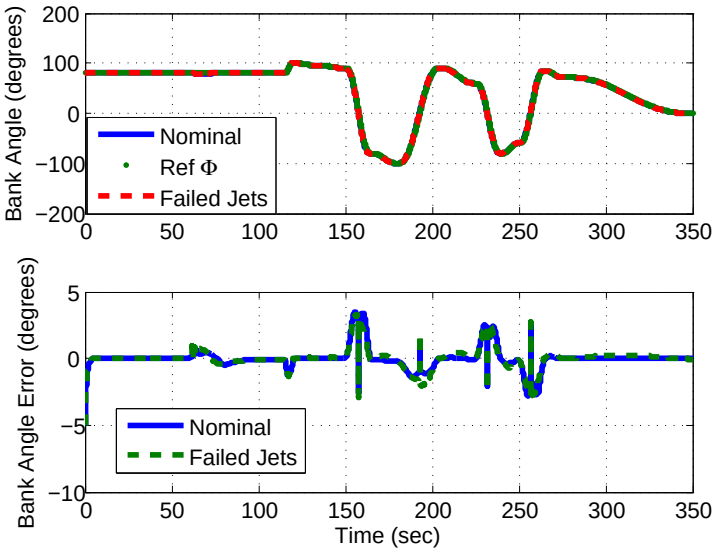

Fig. 11. Test Case 1, Bank Angle and Bank Angle Error

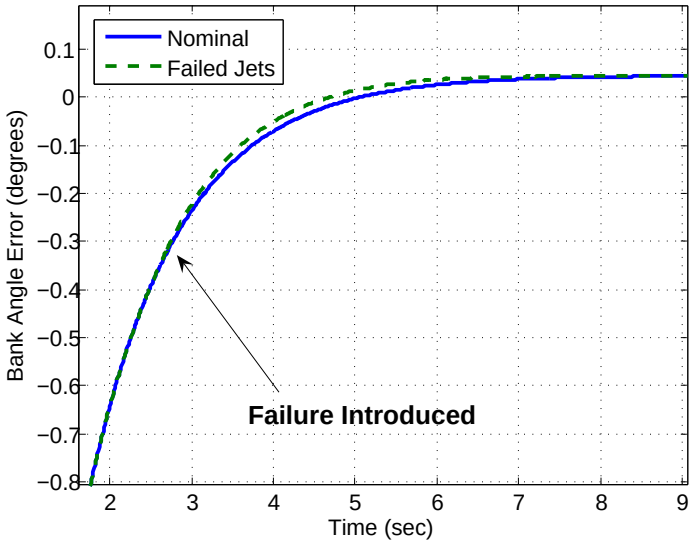

Fig. 12. Test Case 1, Bank Angle Error Response Due To Failure Injection

Figure 13 shows the error in angular velocity about all the three axis. It is observed that the failure does not affect the angular velocity much about roll and yaw axis but it has some effect on the angular velocity about pitch axis. It can be observed that there are some oscillations in angular velocity about pitch axis. These oscillations result due to PWM but the magnitude of these oscillations is of the order 10^{-3}.

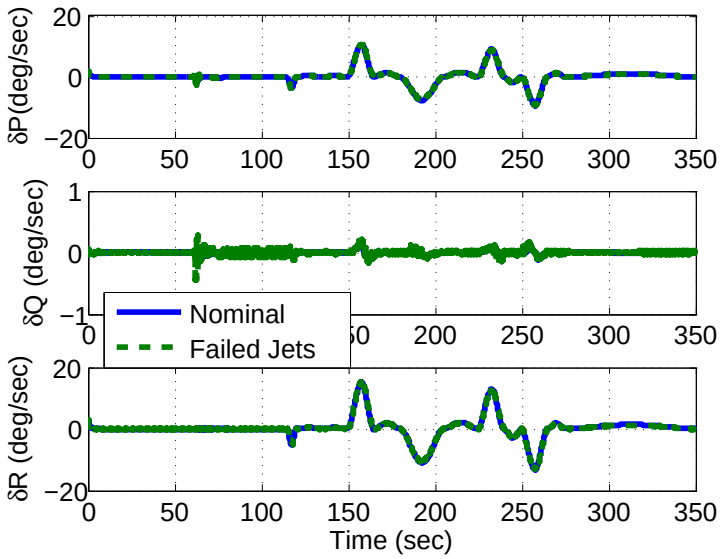

Fig. 13. Test Case 1, Errors in Angular Velocity

Figure 14 shows the errors in the MRPs. It is observed in the following figure that the errors are more in MRPs during the bank angle reversals as compared to the rest of the trajectory. Also since angular velocity is related to the MRPs through a nonlinear transformation matrix $J(\sigma)$, it is expected that the error will occur in the MRPs also. The second parameter has more error than the first and last parameters due to failure injection.

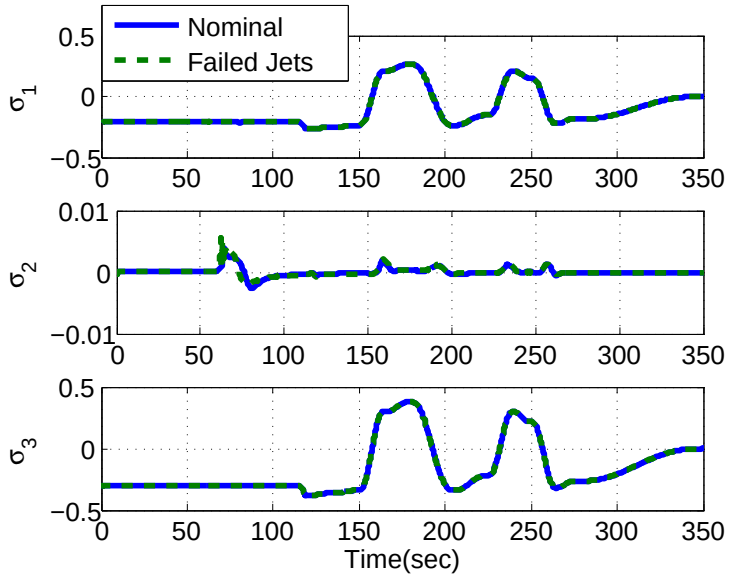

Fig. 14. Test Case 1, Errors in Modified Rodrigues Parameters

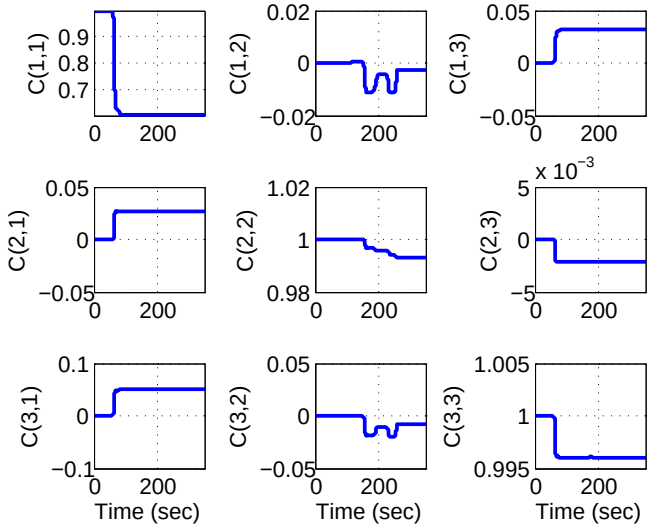

Fig. 15. Test Case 1, Elements of Adaptive Gain C Matrix

Figure 15 shows the elements of adaptive gain matrix C. These adaptive parameters converge to constant values quickly, even though these constant values might not be their true values. Nevertheless, these constant values result in good tracking performance of the system. Similar observations can be made from Figures 16 and 17 which show the elements of adaptive gain matrices D and E respectively. These matrices handle uncertainties in B matrix and failure.

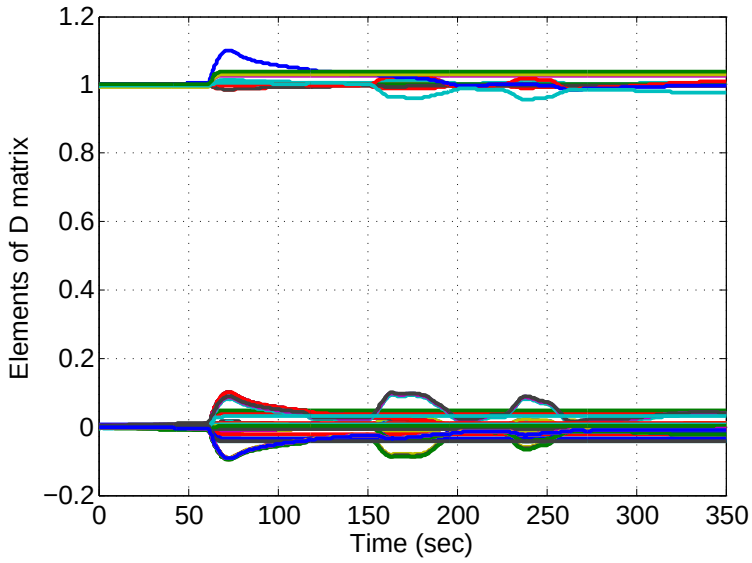

Fig. 16. Test Case 1, Elements of Adaptive Gain D Matrix

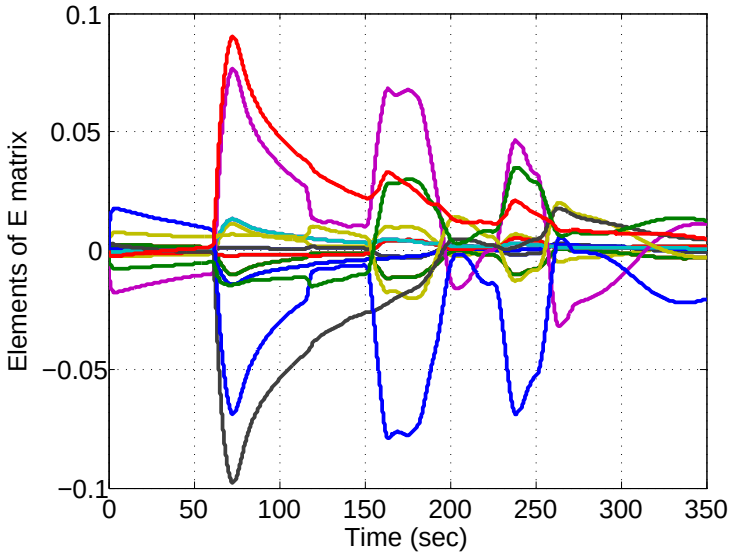

Fig. 17. Test Case 1, Elements of Adaptive Gain E Matrix

Figure 18 shows the translational states of the system. γ and velocity do not depend on control or any other rotational state of the system and hence it is expected that except β, all the other states should be exactly the same for both the nominal as well as the failed jet case(s). However, from the figure it is evident that the velocity and γ values do not match for the two cases,namely, the nominal and the failed jet case. It is due to the fact that, Euler integration is used to integrate the equations of motion and due to different time steps, which are determined by the width of the pulse, there is a slight difference between the two cases.

Although the instantaneous values of the altitude and the downrange are different for the nominal and the failed jet cases, the slope of the trajectory is almost the same in both the cases. This is evident from Figure 19. This implies that the descent rate for the vehicle is almost equal for the two cases.

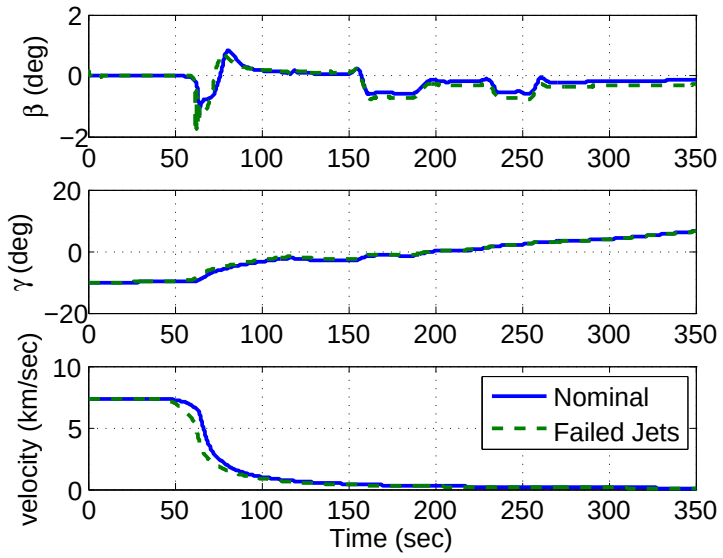

Fig. 18. Test Case 1, Translational States

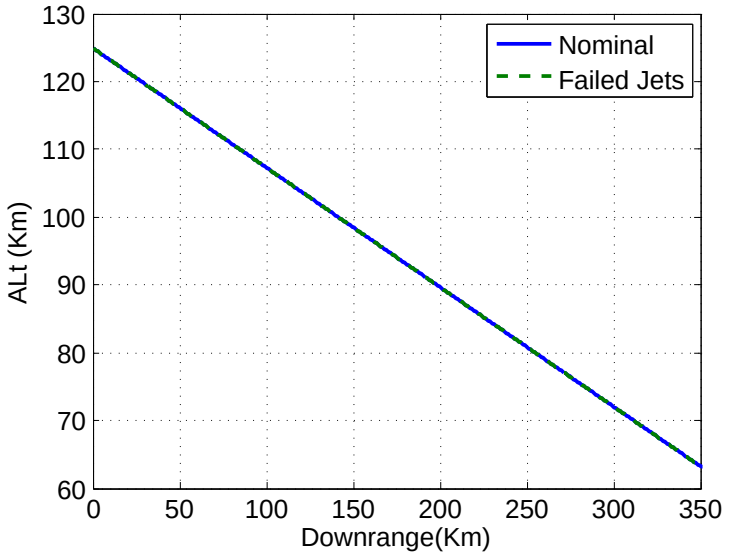

Fig. 19. Test Case 1, Altitude v/s Downrange

2. Test Case 2

In Test Case 2, jets 1, 2, 3, 5, 10, 12, 15, 17 and 18 are failed i.e these jets are always on and produce negative moment. Figures 20 and 21 show the jets after failure introduction. All the failed jets are always on and provide negative moment in this case.

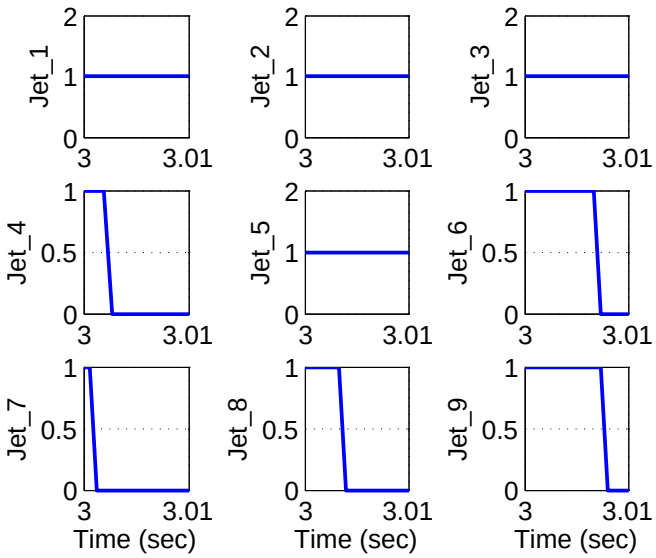

Fig. 20. Test Case 2, RCS Jets (1-9)

Figure 22 shows the error in bank angle trajectory. It can be observed from figure that bank angle error is more mainly during the bank reversals for the failed jet case as compared to the nominal case. Though bank angle is greater, it is well within the range. The maximum error in the bank angle for the failed case is ± 5 *degrees*. Figure 22 shows that controller is able to handle the jet failures and bring the error to zero.

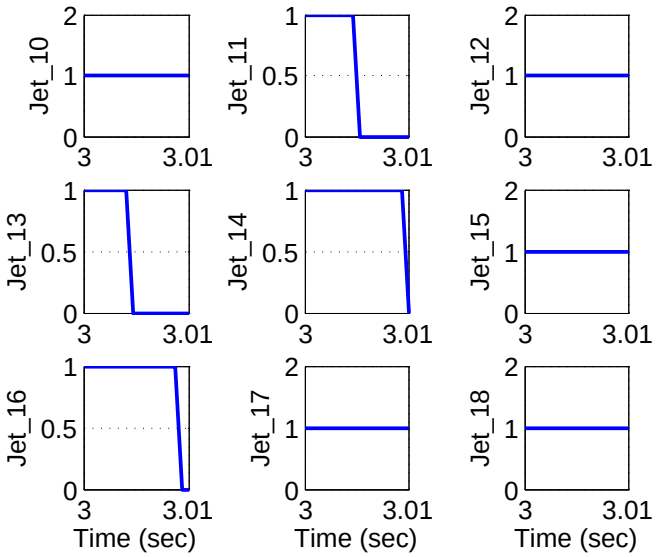

Fig. 21. Test Case 2, RCS Jets (10-18)

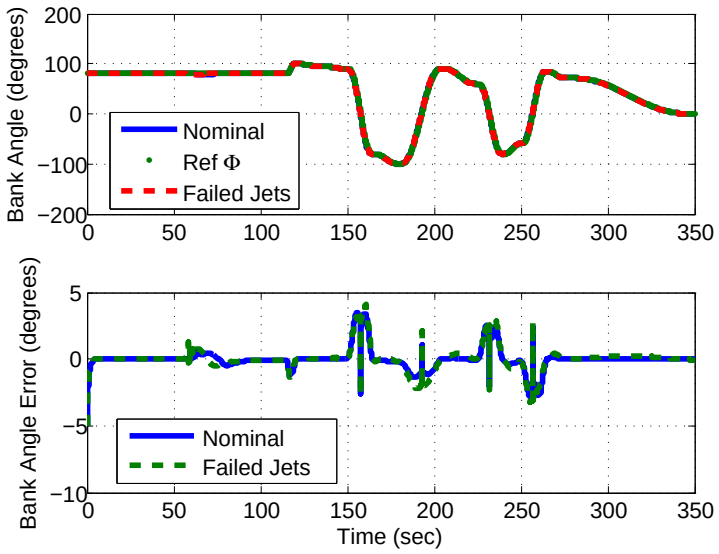

Fig. 22. Test Case 2, Bank Angle and Bank Angle Error

Failure is introduced at 2.5 seconds, Figure 23 shows that trajectory for bank angle will change after failure is introduced. Fault Tolerant SAMI recalculates the control so that it should follow the reference trajectory with minimum error.

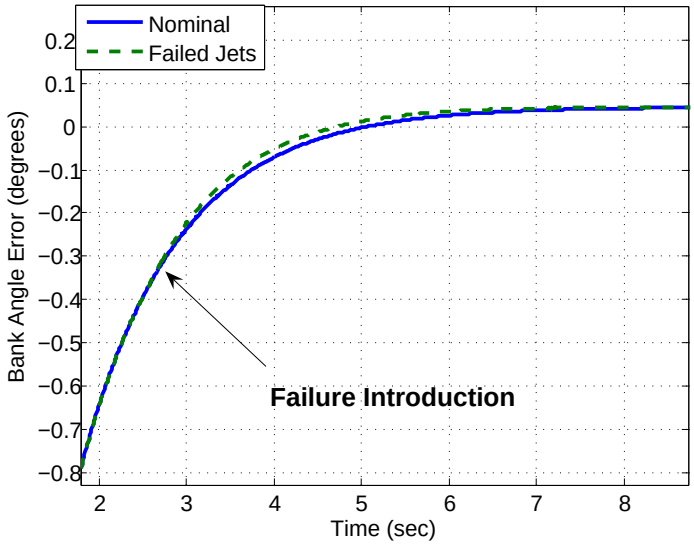

Fig. 23. Test Case 2, Bank Angle Error Response Due To Failure Injection

Figure 24 shows the three components of the angular velocity. As was observed in Test Case 1, the angular velocity component along pitch axis has oscillations of negligible magnitude for the case of jet failure. It is therefore evident from the figure that the controller is able to track not only the kinematic states but also the dynamic states of the vehicle.

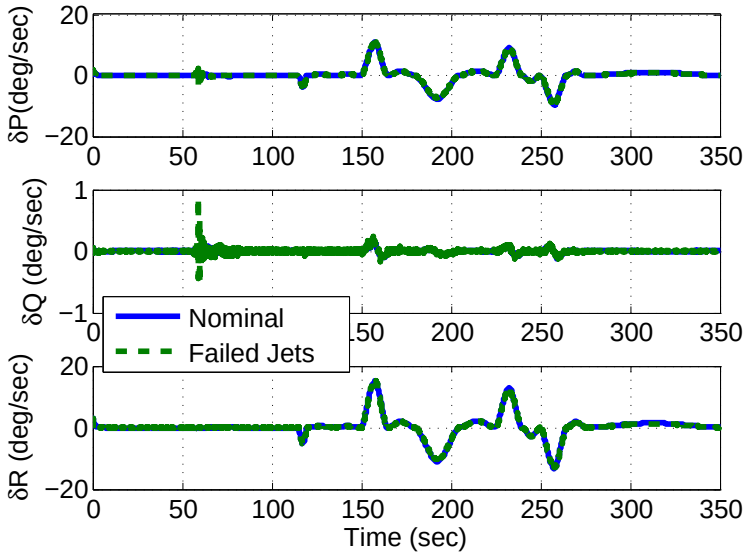

Fig. 24. Test Case 2, Errors in Angular Velocity

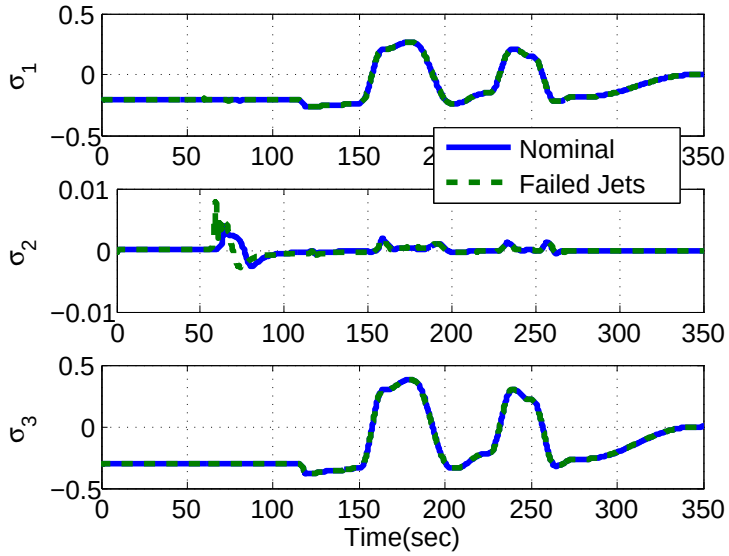

Fig. 25. Test Case 2, Errors in Modified Rodrigues Parameters

Figure 25 shows that the error in MRPs is slightly more in the case of failed jets than in the nominal case. Also, the reduction in the error in all the MRPs to zero manifests that the controller can reconfigure itself and is able to handle the jet failure.

All the adaptive parameters i.e. elements of C, D and E matrices are shown below in Figures 26, 27 and 28. Using the update laws derived in Chapter II, these parameters are updated and used in the control laws. Based on the earlier discussion, it can be concluded that the control law calculated using these parameters results in good tracking performance.

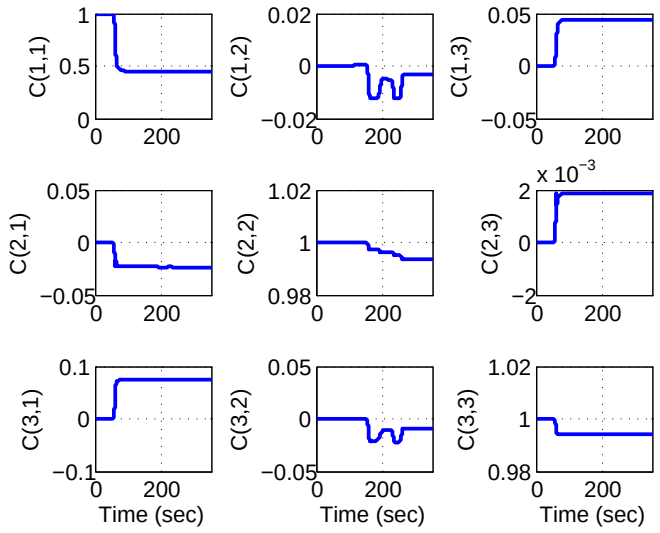

Fig. 26. Test Case 2, Elements of Adaptive Gain C Matrix

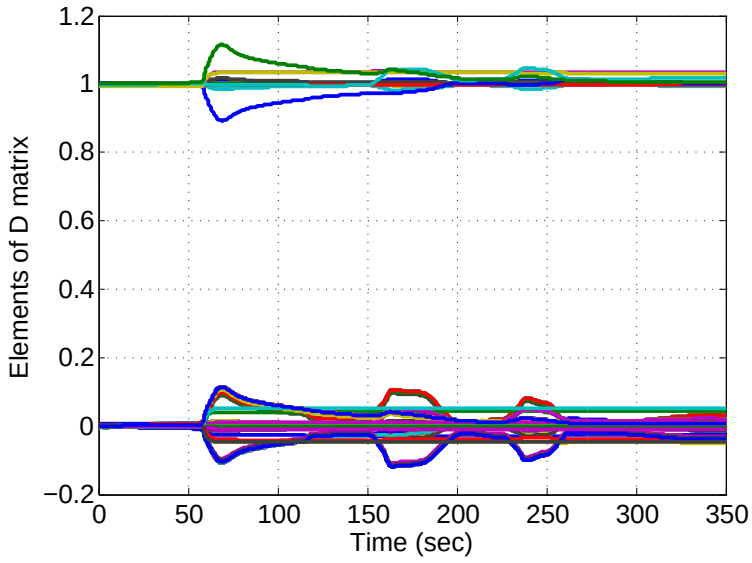

Fig. 27. Test Case 2, Elements of Adaptive Gain D Matrix

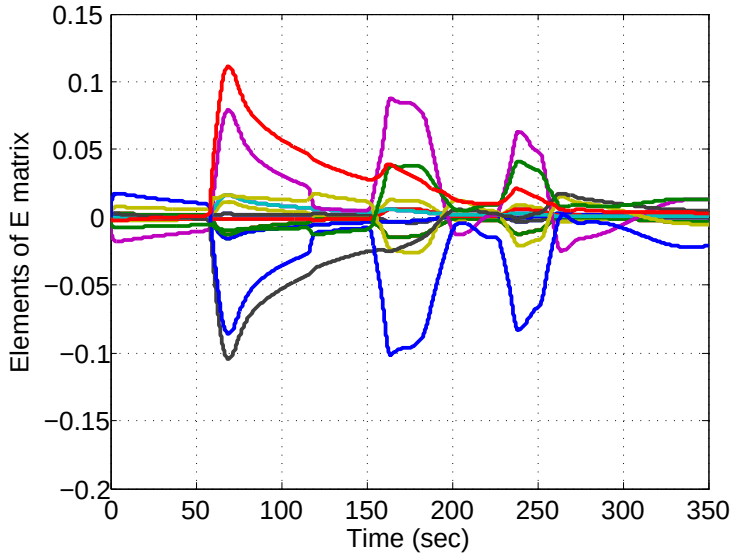

Fig. 28. Test Case 2, Elements of Adaptive Gain E Matrix

Figure 29 shows the time histories of the translational states for the Test Case 2. The states settle down to slightly different values for the failed and the nominal case. On comparison with the previous case, it can be inferred that the translational states are very similar for the two cases.

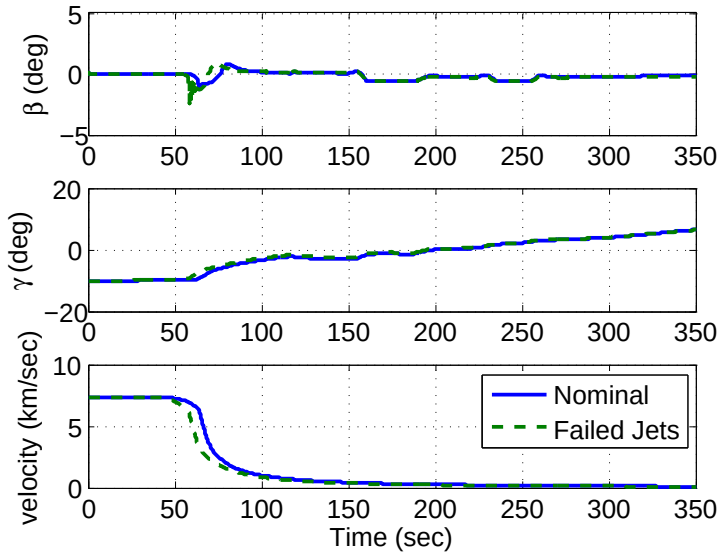

Fig. 29. Test Case 2, Time Histories of Translational States

Figure 30 shows the altitude versus downrange plot for the present case.

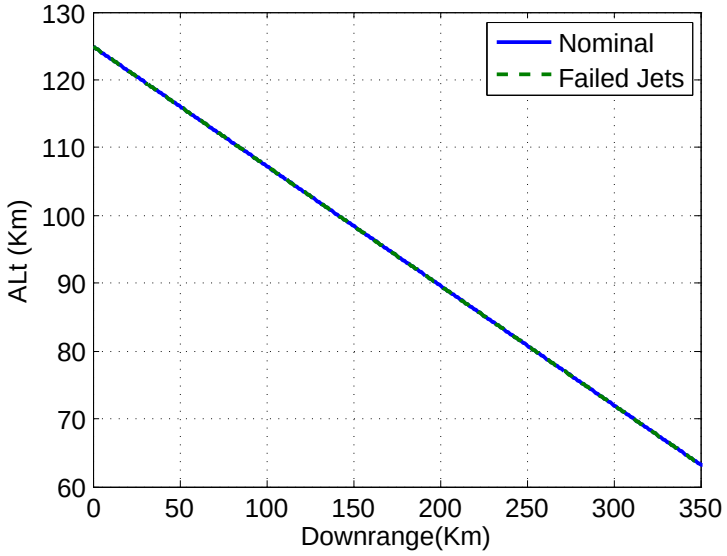

Fig. 30. Test Case 2, Altitude v/s Downrange

B. Results for Fault Tolerant Control Allocation Controller

1. Test Case 3

In Test Case 3 jets 1, 2, 17 and 18 are considered inoperable such that they do not provide thrust after 2.5 seconds as shown in Figures 31 and 32. These discrete jets can only take the binary value of 1 or 0. As shown in the plots, once the failure is introduced, the numerical value for the failed jets is 0 and this implies that they are off.

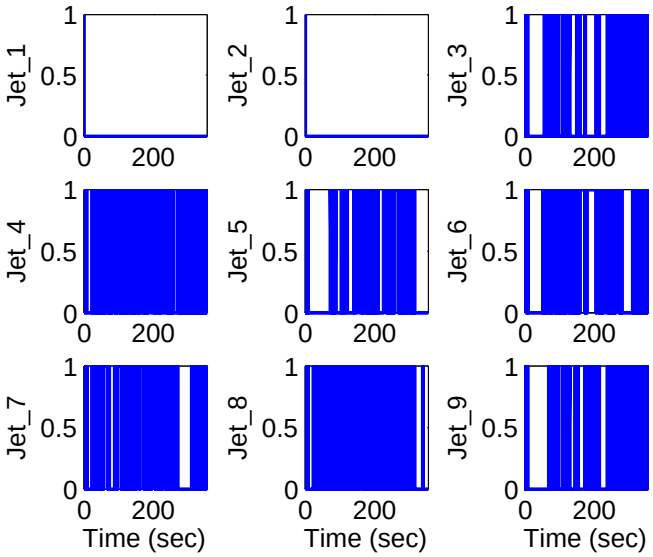

Fig. 31. Test Case 3, RCS Jets (1-9)

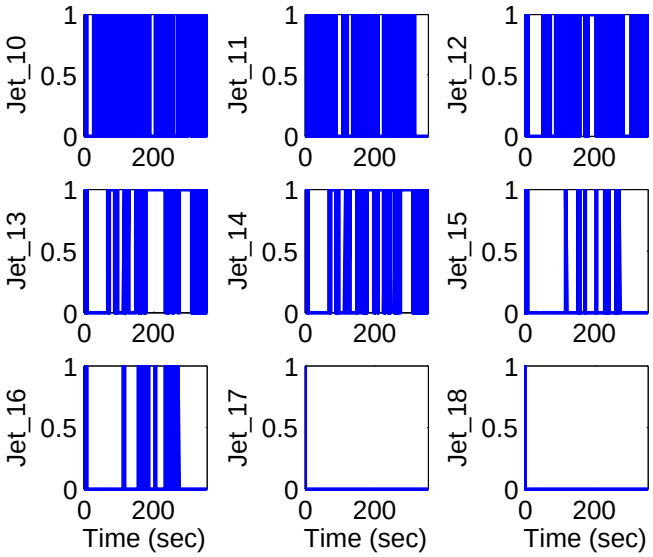

Fig. 32. Test Case 3, RCS Jets (10-18)

By comparing the failed jet response to the nominal case, as shown in Figure 33, it is observed that as soon as the failure is introduced, the tracking performance degrades and the settling time increases. However the system is able to regulate the tracking error to near zero values within the first few seconds after the failure is introduced. Also, whenever the bank angle reversal occurs, the error is greater in the failed jet case than in the nominal case.

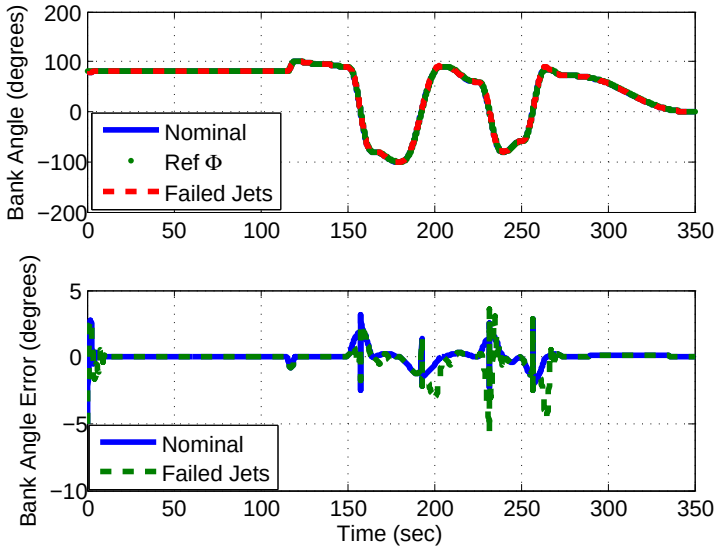

Fig. 33. Test Case 3, Bank Angle and Bank Angle Error

Figure 34 shows the effect of the initial condition error on the bank angle response and the failure. The initial condition error makes the tracking difficult, but the controller is able to handle the failure too.

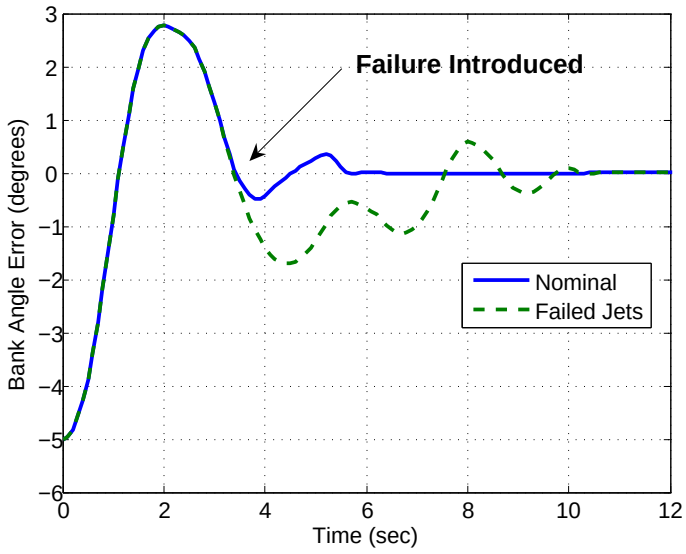

Fig. 34. Test Case 3, Bank Angle Error Response Due To Failure Injection

The controller is also designed to track the reference angular velocities. Figure 35 compares the error in the three angular velocity components for Test Case 3 and the nominal case, and shows the ability of the controller to track the reference angular velocities.

The MRPs (kinematics state) for Test Case 3 also follow the reference MRPs as shown in the Figure 36. The errors in all three components of the MRP vectors show that the failed jets have more of an adverse effect on the second component of the MRP vector, and hence it takes more time to follow the reference vector as compared to the other two components.

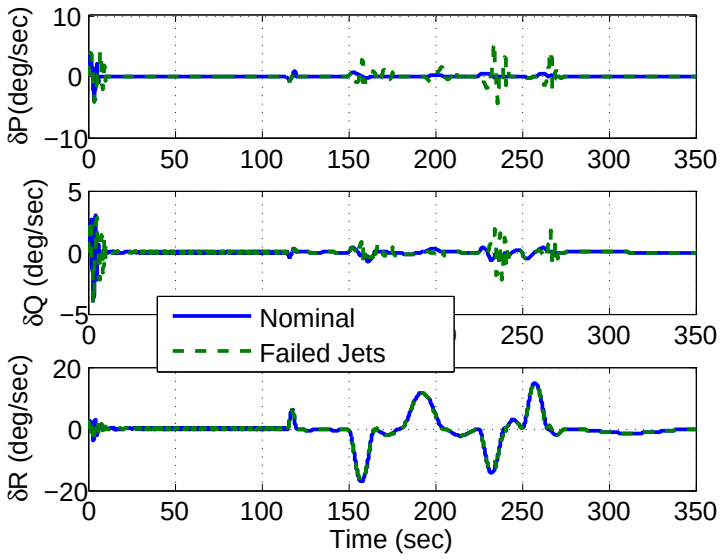

Fig. 35. Test Case 3, Errors in Angular Velocity

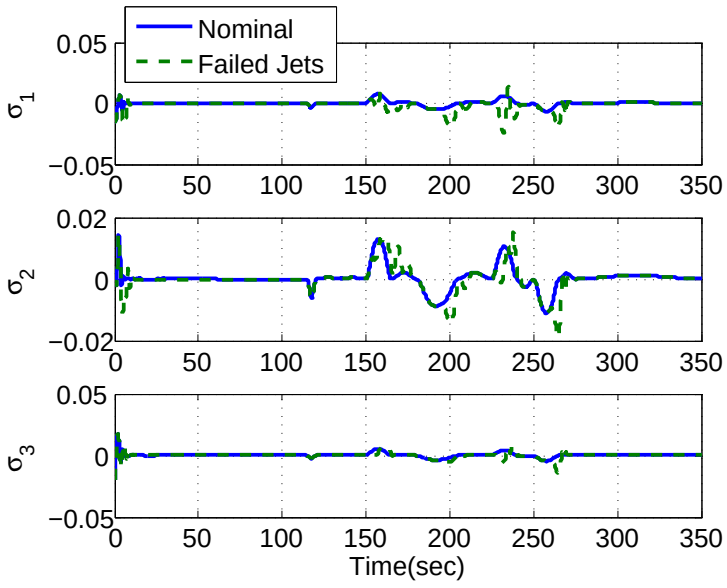

Fig. 36. Test Case 3, Errors in Modified Rodrigues Parameters

Due to the jet failure some of the jets are not participating in tracking the reference trajectory. This is equivalent to a situation in which the moment produced by the jets is less than the nominal case, resulting in more tracking error as compared to the nominal case. To reduce this error the commanded and hence applied control is greater in the case of the failed jets. Time histories of the commanded control and the applied control are shown in Figures 37 and 38 respectively. It is evident from Figure 38 that the applied control in failed case is greater than the nominal case.

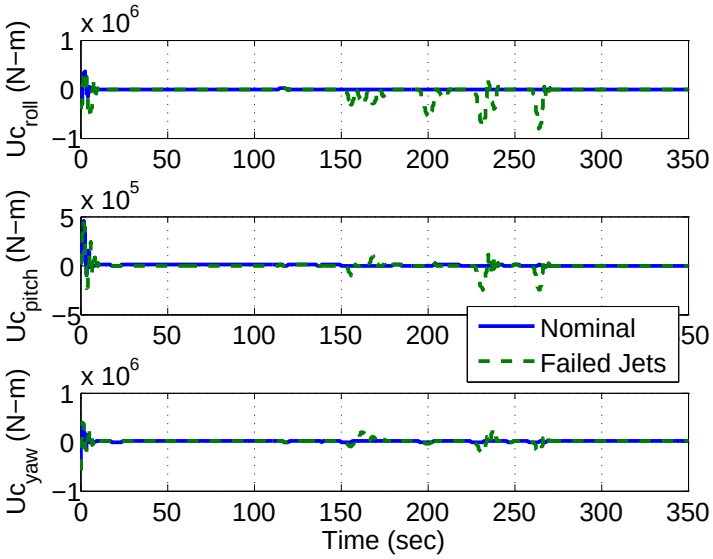

Fig. 37. Test Case 3, Commanded Control

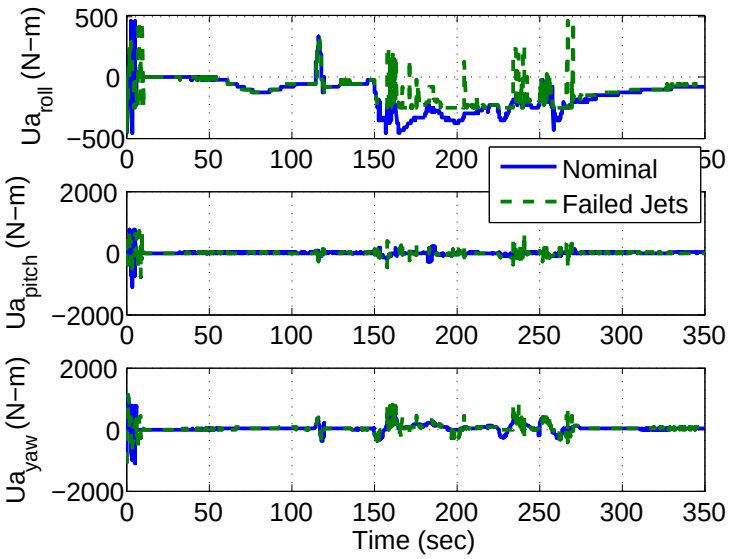

Fig. 38. Test Case 3, Applied Control

The adaptive controller performs as expected and updates both the inertia vector and d vector as shown in Figures 39 and 40. All of the adaptive parameters converge to constant values as defined by the update laws. How fast the adaptive parameters converge to a constant value depends upon the gain matrix.

The translational states β, γ, and velocity are shown in Figure 41. Since the equations for velocity and γ do not depend on rotational states and control, they are exactly the same for both the nominal and failed jet cases. β changes with the failure of jets and therefore settles down at a slightly different value.

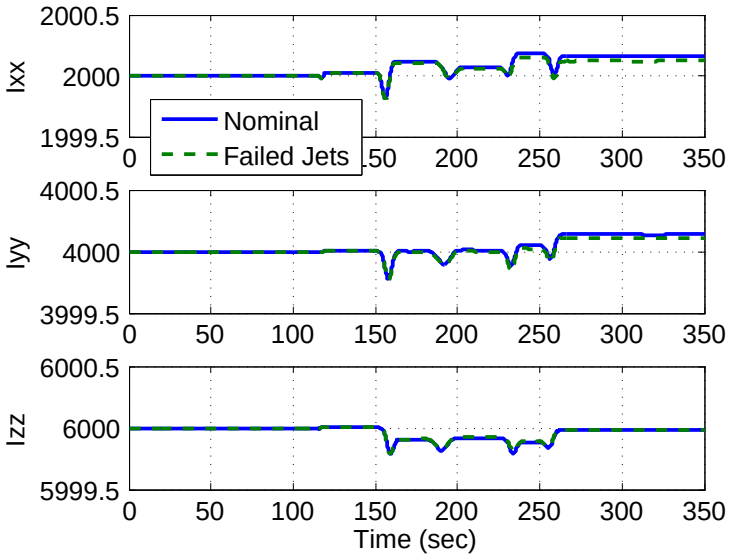

Fig. 39. Test Case 3, Elements of Inertia Matrix

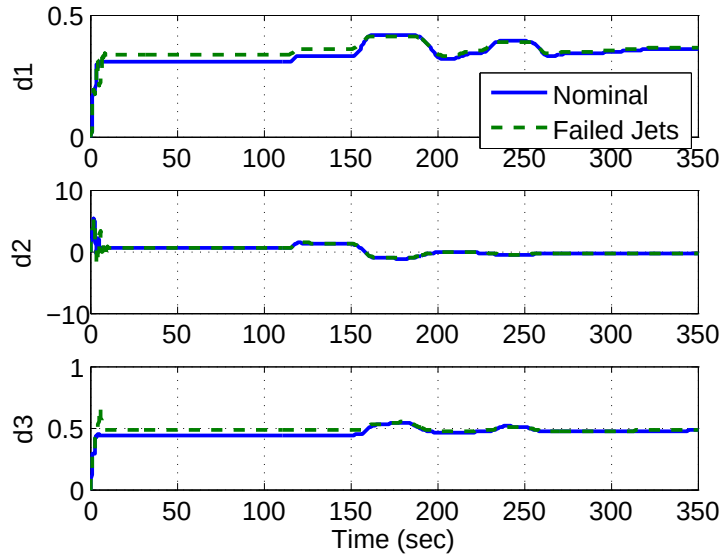

Fig. 40. Test Case 3, Adaptive Parameters

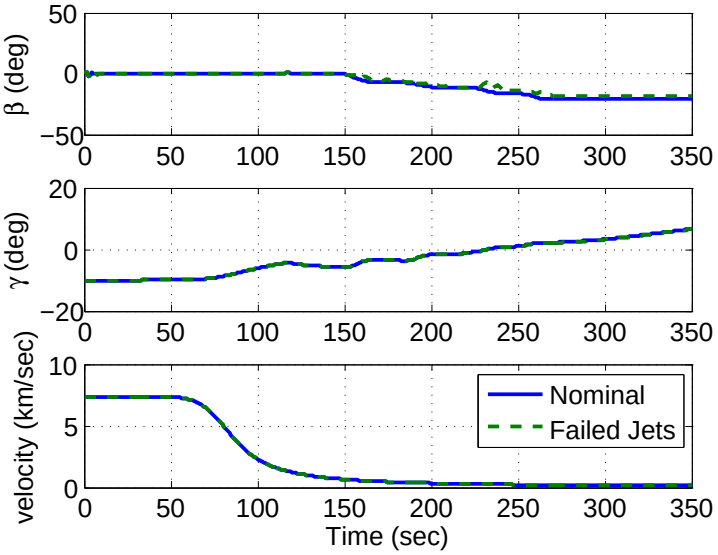

Fig. 41. Test Case 3, Translational States

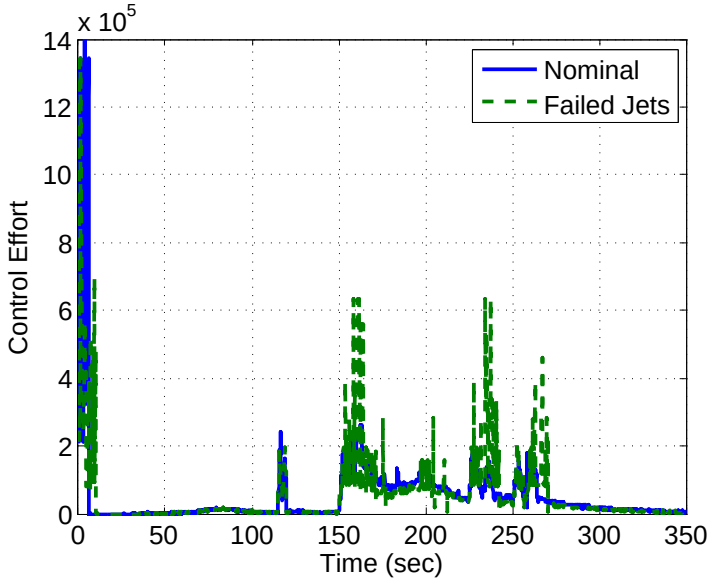

Fig. 42. Test Case 3, Control Effort

It was observed earlier that the commanded and the applied control are greater in the case of failed jets. Therefore, it is expected that control effort, defined as $u^T u$, is greater in the case of failed jets. Figure 42 shows the control effort and as expected, the required control effort is greater in the failed jet case than in the nominal case. In summary, the results of Test Case 3 demonstrate that failed jets can be easily handled by the combined adaptive control and Fault Tolerant Control Allocation scheme.

In the plot of altitude versus downrange trajectory in Figure 43, the vehicle is seen to lose altitude at the same rate in both simulations.

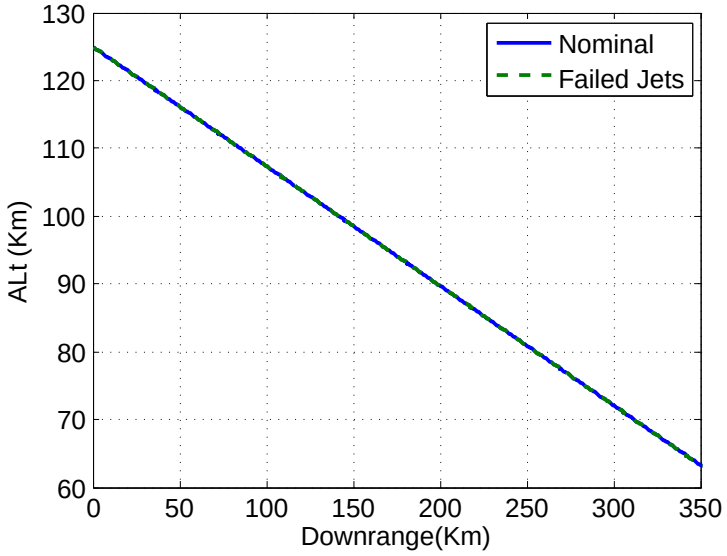

Fig. 43. Test Case 3, Altitude v/s Downrange

In summary, the results of Test Case 3 demonstrate that failed jets can be easily handled by the combined adaptive control and Fault Tolerant Control Allocation scheme.

2. Test Case 4

For Test Case 4 some of the jets are always on. Due to this failure a moment is continuously generated in a particular direction. Figures 44 and 45 show that jets 2, 3, 4, 5, 8, 9 and 10 are always on after 2.5 seconds and produce thrust continuously.

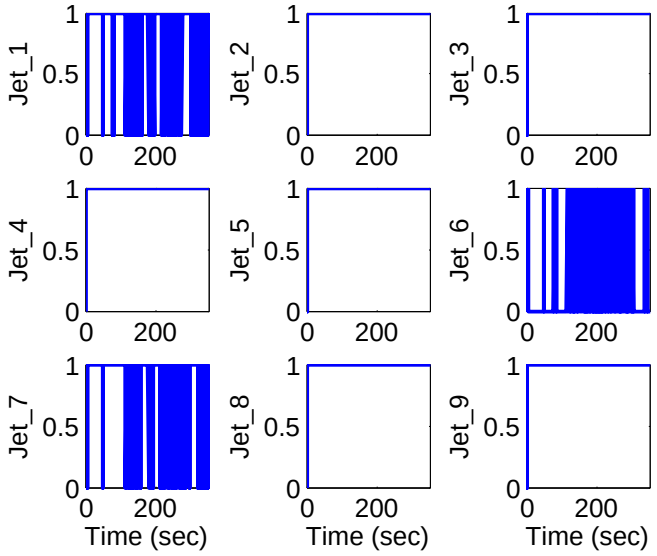

Fig. 44. Test Case 4, RCS Jets (1-9)

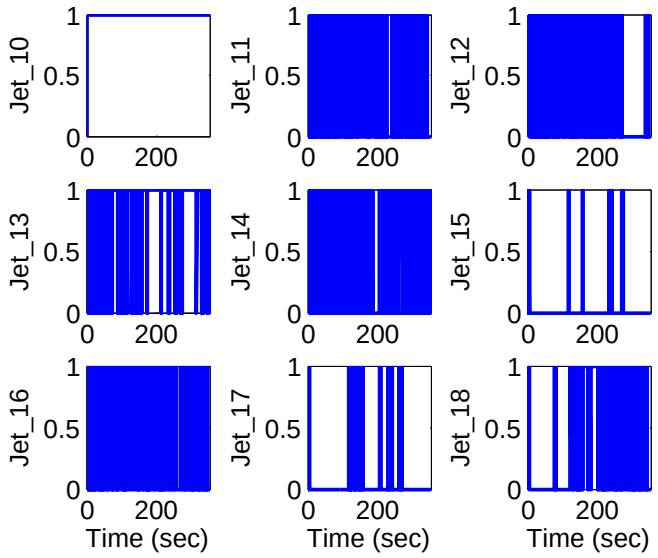

Fig. 45. Test Case 4, RCS Jets (10-18)

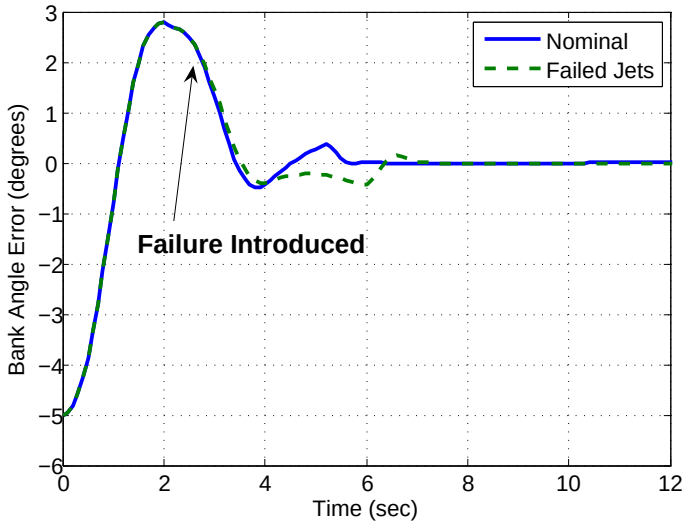

Fig. 46. Test Case 4, Bank Angle Error Due To Injection of Failure

Figure 46 shows the effect of the initial condition error in bank angle, and the introduction of the failure. The error on Φ increases as expected due to the error in the initial condition, yet the algorithm efficiently handles both the initial condition error and the failure at the same time.

Figure 47 shows the error in bank angle for the complete trajectory. The error is greater than the nominal case, but the controller is able to handle the error not only during the constant command, but also during the bank angle reversals.

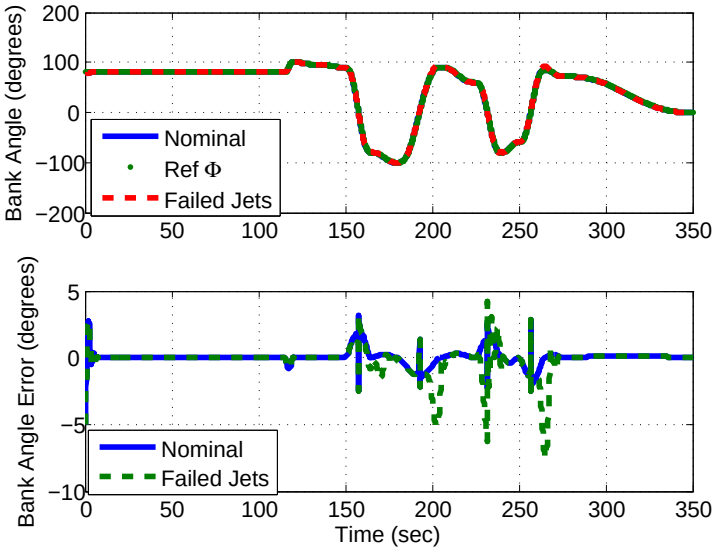

Fig. 47. Test Case 4, Bank Angle and Bank Angle Error

Figure 48 shows the time histories of errors in the MRPs and also compares the MRPs in Test Case 4 to those of the nominal case. As expected the error in the MRPs is greater compared to the nominal case MRPs. It is observed from Figure 48 that all three components of the MRPs show greater error during the bank angle reversals in the case of failed jets.

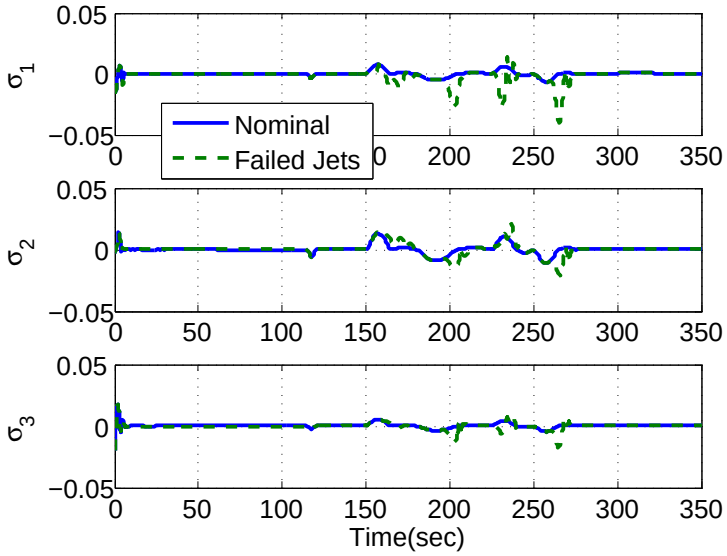

Fig. 48. Test Case 4, Errors in Modified Rodrigues Parameters

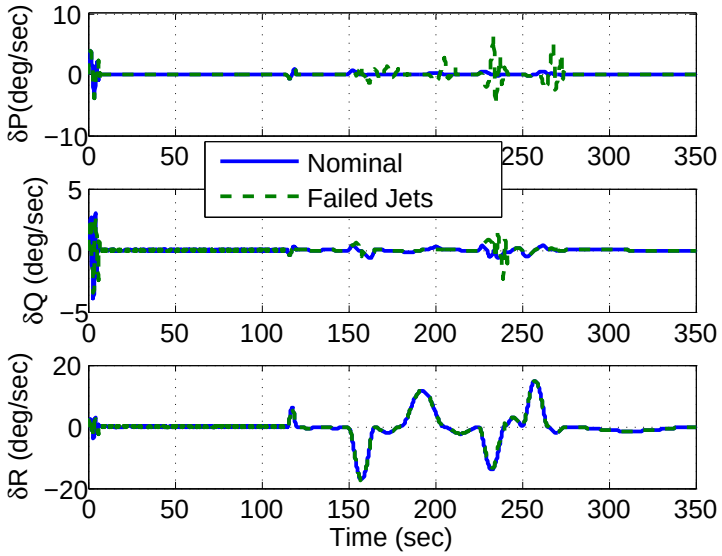

Fig. 49. Test Case 4, Errors in Angular Velocity

The controller is seen to handle not only the kinematic but also the dynamic state errors during this kind of failure. It is clear from Figure 49 that this failure resulted in greater errors about the roll and pitch axis, but not much less about the yaw axis.

The inertia vector and d vector are updated based on the adaptive laws derived earlier. It is shown in Figures 50 and 51 that although these adaptive parameters may not converge to their original value, they do converge to a constant value which results in a control signal which is able to track the reference trajectory.

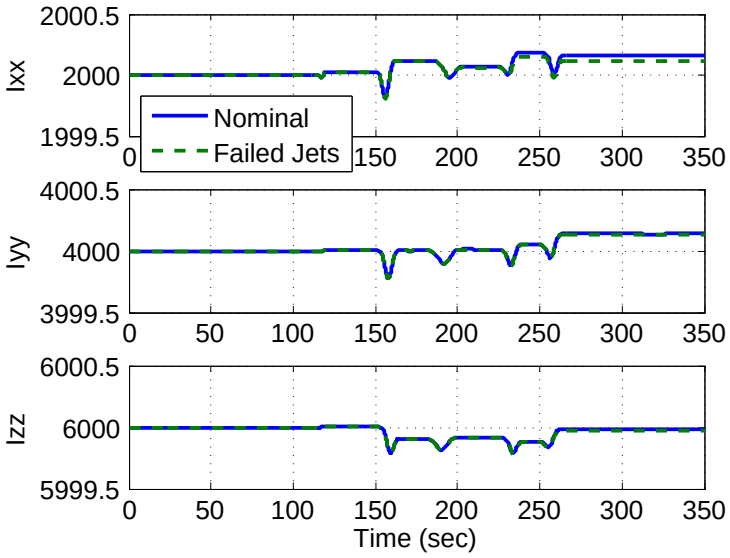

Fig. 50. Test Case 4, Elements of Inertia Matrix

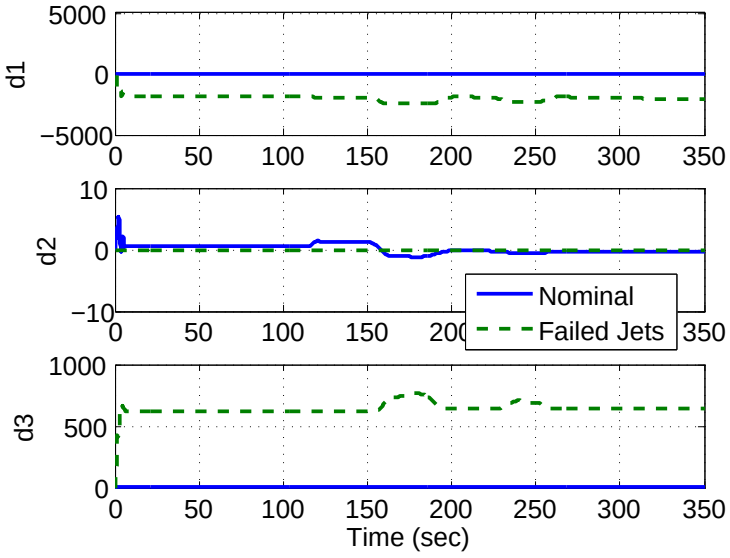

Fig. 51. Test Case 4, Adaptive Parameters

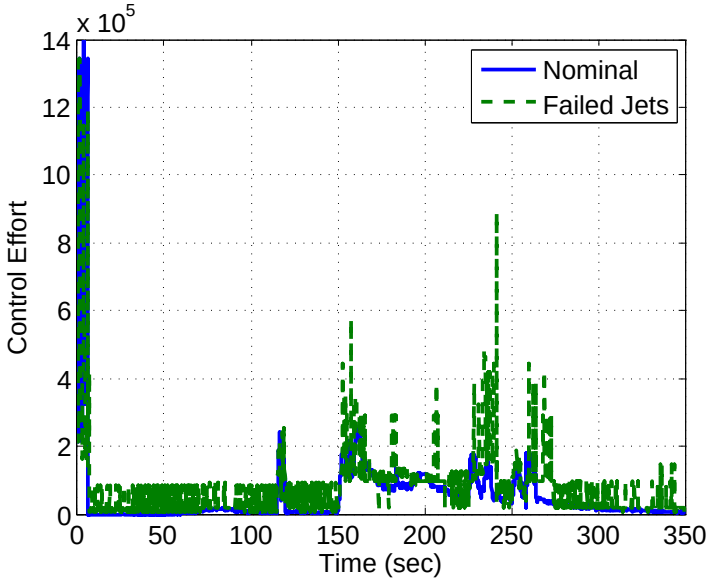

Fig. 52. Test Case 4, Control Effort

Figure 52 shows the control effort. As expected the control effort required is greater in this case as compared to the nominal case. As seen from Figures 48 and 49 the error in both the dynamic and kinematic level states is greater for the case of jet failure as compared to the nominal case, and hence more control effort is required to reduce this error over time. Due to greater tracking errors the controller will command more control effort. The control allocation algorithm solves this problem by supplying more control according to the given constraints.

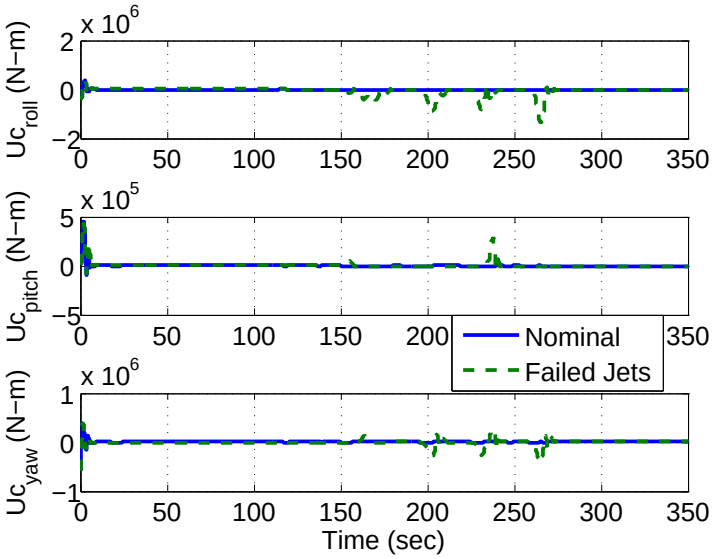

Fig. 53. Test Case 4, Commanded Control

Time histories of the commanded and applied control are shown in Figures 53 and 54. It can be seen that in the case of failed jets the commanded and hence applied control is large. Comparison of the translational states β, γ and velocity are shown in Figure 55. As explained in Test Case 3, it is expected that in the failed jet case β will settle down at a different value than the nominal case. The other translational states do not depend on rotational states or control directly, and hence will be exactly the same for both cases.

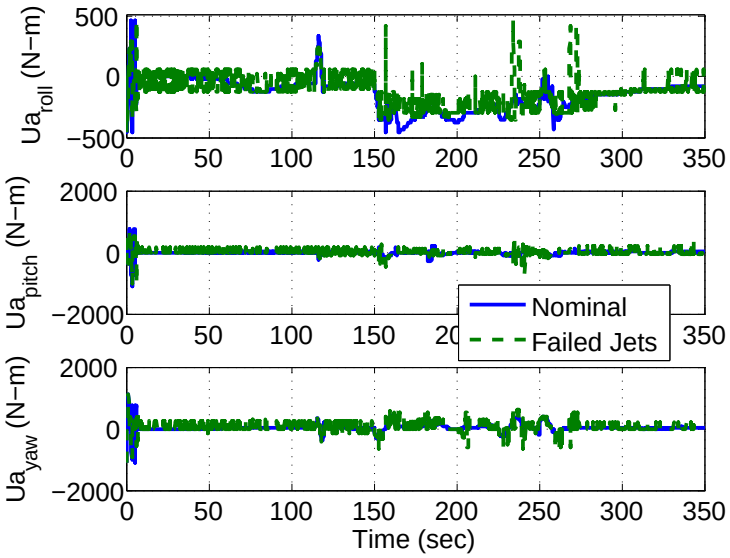

Fig. 54. Test Case 4, Applied Control

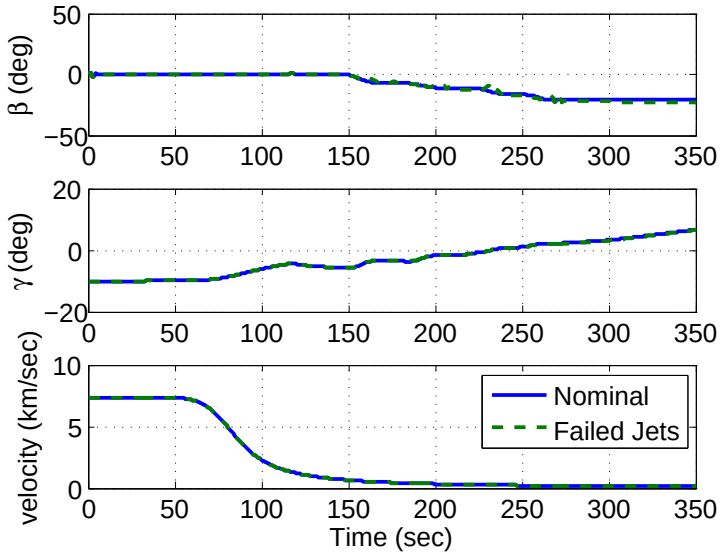

Fig. 55. Test Case 4, Time Histories of Translational States

Figure 56 shows the altitude versus downrange.

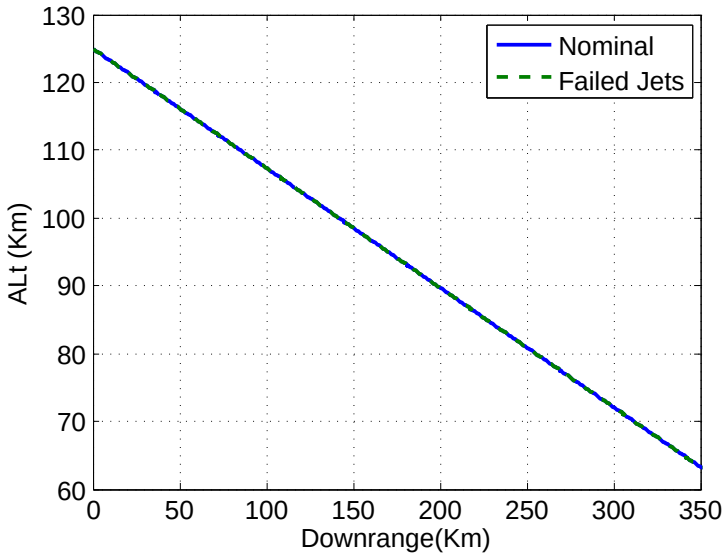

Fig. 56. Test Case 4, Altitude v/s Downrange

3. Test Case 5

Test Case 5 assumes that the thrust producing capacity of certain jets is diminshed. Instead of producing torque equal to the constants given in matrix A in the Appendix A, some of the jets produce less thrust. Figure 57 shows that the error due to the bank angle initial condition gets added to the error due to the jet failures at 2.5 seconds, resulting in a larger error during the first few seconds of the trajectory. The simulation results demonstrate that the algorithm handles these errors well.

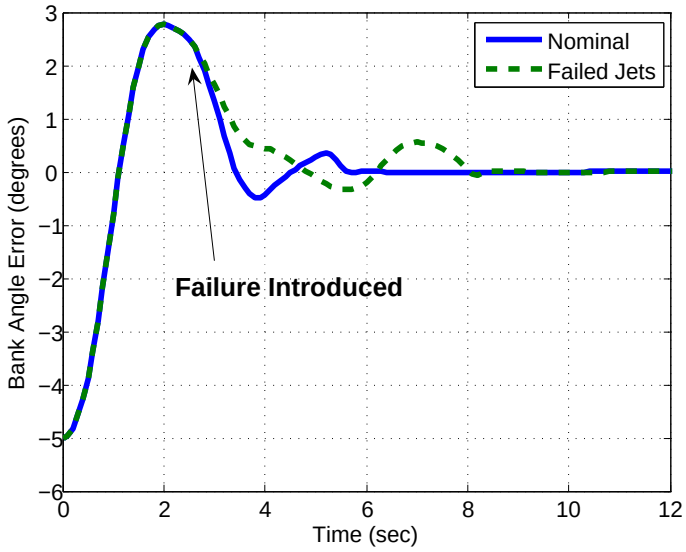

Fig. 57. Test Case 5, Bank Angle Error Response Due To Injection of Failure

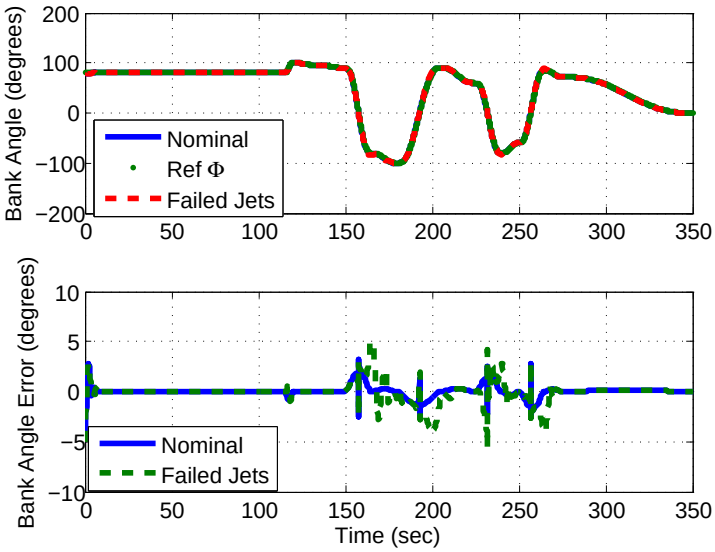

Fig. 58. Test Case 5, Bank Angle and Bank Angle Error

In Figure 58 the error in the bank angle trajectory is shown for the complete trajectory. As seen in Test Cases 3 and 4 this type of failure also produces large errors, but the controller is able to handle them and reduces the tracking error. Comparison of the errors in Test Case 5 with the nominal case in Figures 59 and 60 show that both the kinematic and dynamic level states indicated differences in the two cases. Time histories of the error show that jet failure produces more error in all of the states.

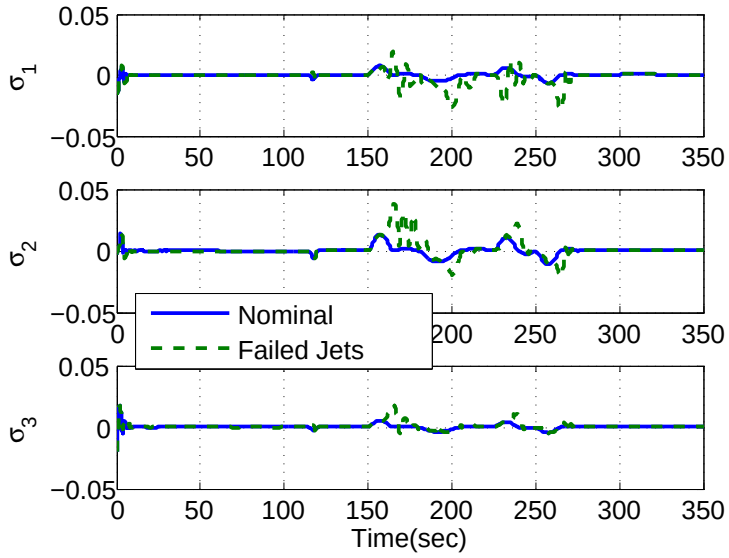

Fig. 59. Test Case 5, Errors in Modified Rodrigues Parameters

Failure of jets will result in angular velocity errors about all three axes due to the assumption that each jet contributes torque in all three directions. Errors in angular velocity components δP, δQ and δR are shown in the Figure 60 and it is seen that using the Fault Tolerant Control Allocation the working jets are able to reduce the error in all three components.

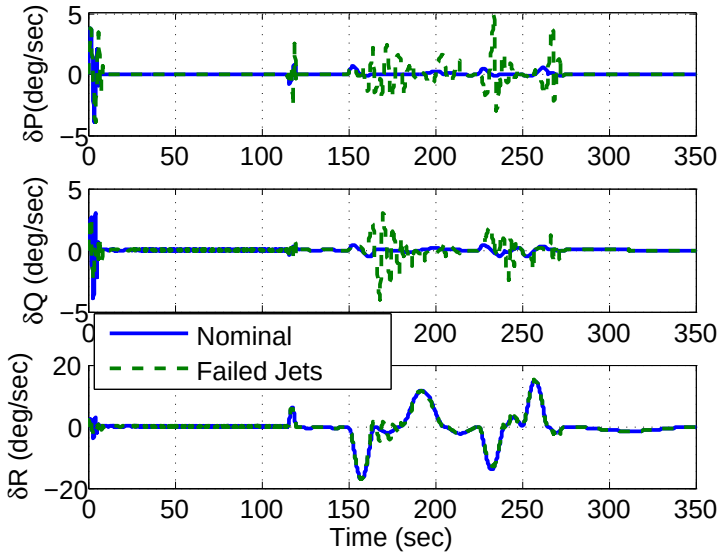

Fig. 60. Test Case 5, Errors in Angular Velocity

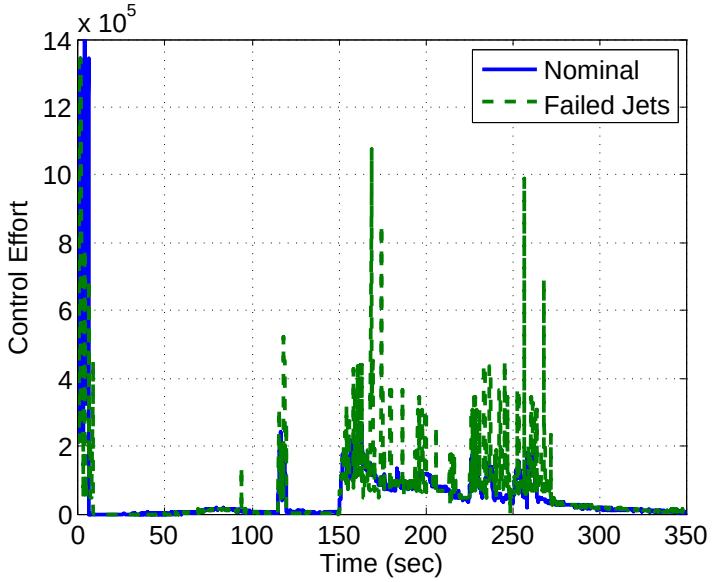

Fig. 61. Test Case 5, Control Effort

Figure 61 shows that when the jets are producing less thrust than their normal output due to a fuel leakage, valve malfunction, or similar failure the controller re-configures and provides sufficient control to reduce the tracking error. The inertia vector and d vector updates are shown in Figures 62 and 63. It is observed that the inertia vectors and adaptive parameters converge to a constant value, which is used in the control laws instead of the uncertain parameters.

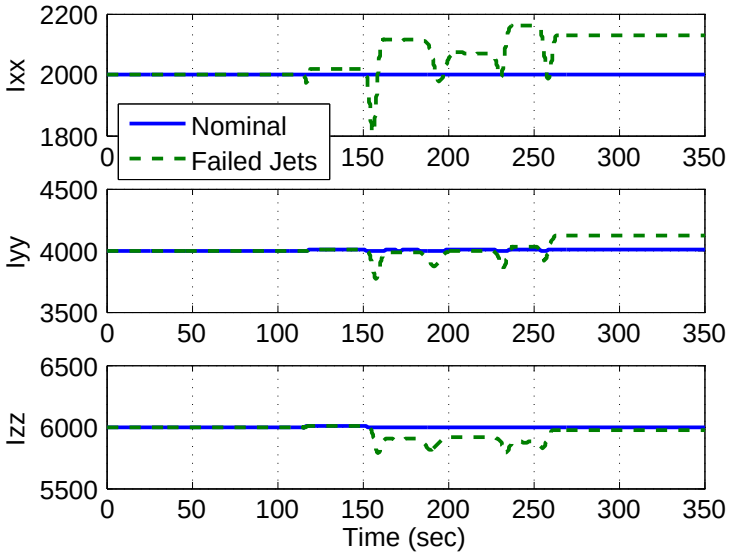

Fig. 62. Test Case 5, Elements of Inertia Matrix

Due to failures more control effort is required to reduce the tracking error. As expected the commanded and hence the applied torque are greater in Test Case 5 than in the nominal case, because of the decreased capacity of the jets to produce thrust. Commanded and applied control is shown in Figures 64 and 65.

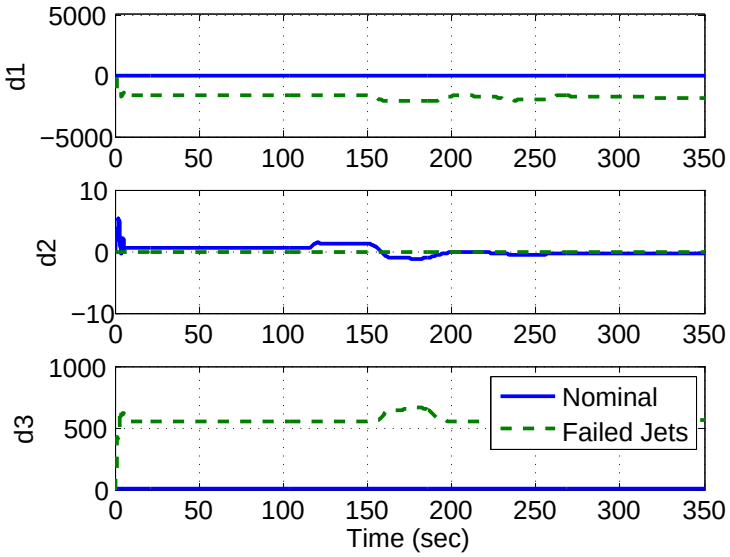

Fig. 63. Test Case 5, Adaptive Parameters

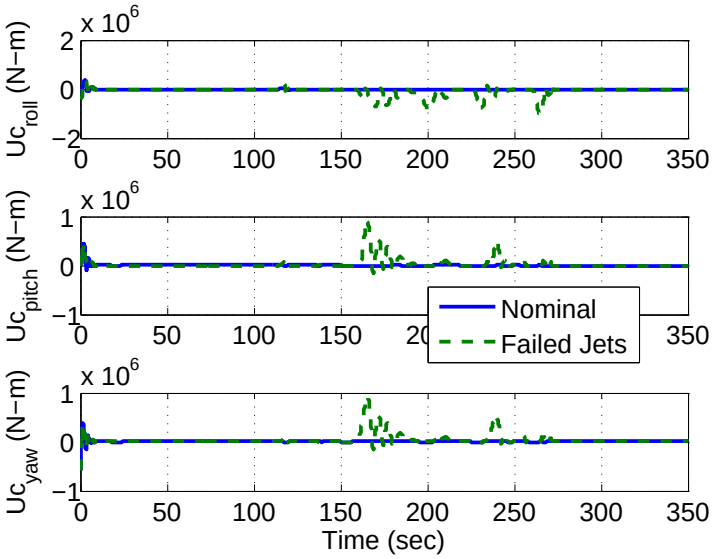

Fig. 64. Test Case 5, Commanded Control

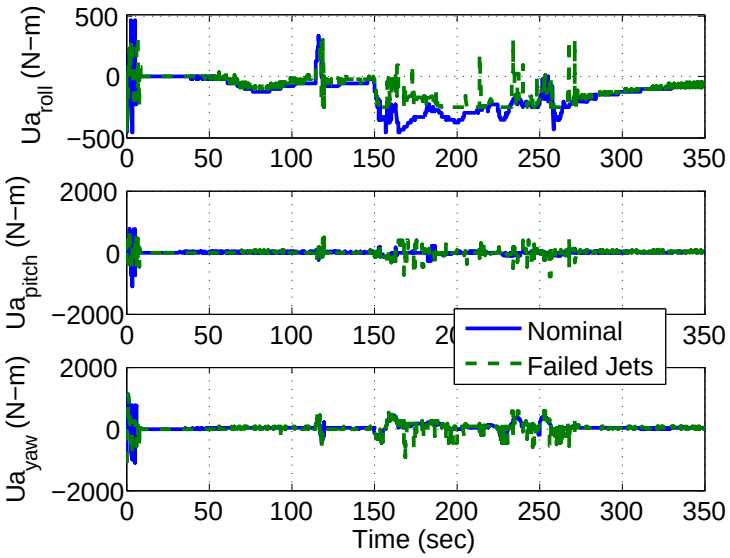

Fig. 65. Test Case 5, Applied Control

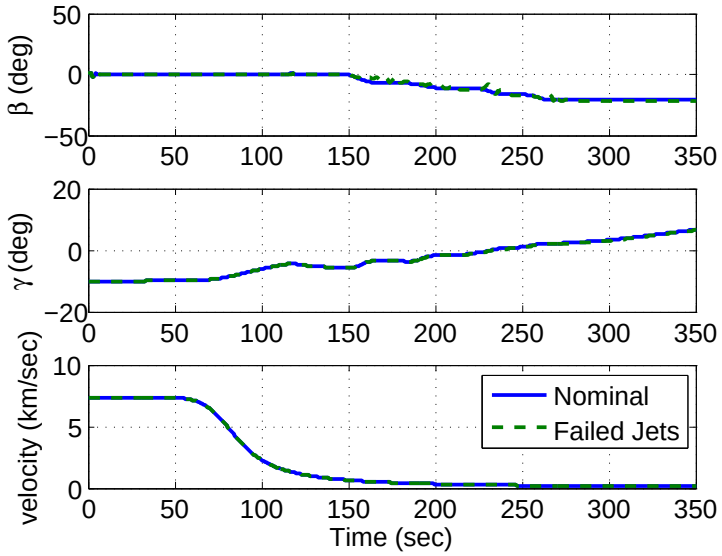

Fig. 66. Test Case 5, Time Histories of Translational States

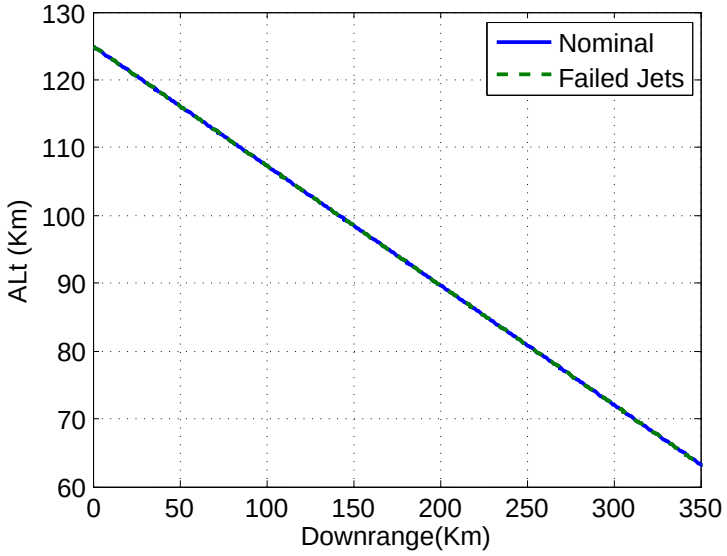

Fig. 67. Test Case 5, Altitude v/s Downrange

Except for β all the translational states are expected to behave alike in both the nominal and jet failure case, and this can be verified from Figures 66 and 67.

CHAPTER VI

CONCLUSIONS

Based on the results presented in this thesis, the following conclusions can be drawn:

1. The Fault Tolerant Structured Adaptive Model Inversion controller successfully handles failures if one or several discrete control effectors fail, or if the efficiency of one or several control effectors decreases. This is demonstrated in the presence of simultaneous initial condition errors and uncertainties in plant and operating environment parameters, without a fault detection scheme. The maximum bank angle error is $\pm$ 5 degrees.

2. The Fault Tolerant Control Allocation controller with discrete control allocation successfully handles failures if one or several jets fail, or if the efficiency of one or several jets decreases. Recovery and re-tracking of reference states and angular velocity is observed after all failures, and the maximum bank angle error due to failures is $\pm$ 5 *degrees*. This controller is able to successfully track both the kinematic and dynamic states during and after failures. The control effort required to track the desired trajectory for the nominal and failed jet cases is greater for the failed jets case, yet trajectory tracking is still within acceptable limits.

3. While the Fault Tolerant Control Allocation controller places no restriction on the magnitude of the desired control, it was observed that large control magnitudes and the non-existence of optimal solutions for a particular case may result. Some control scheme would be needed to handle such situations.

CHAPTER VII

RECOMMENDATIONS AND FUTURE RESEARCH DIRECTIONS

Following recommendations have been made for the future research.

1. The most pertinent extension of this work is to find the Lyapunov function for the nonlinear system to prove the stability using quantized control for the uniformly stable system. Two approaches which were discussed in this thesis can then be extended to prove the stability of such systems.

2. Uncertain coefficients and Mars atmospheric density were combined in this work and were treated as one adaptive parameter. These parameters can be studied more carefully by treating them as separate parameters in mathematical equations as done for moments of inertia in Chapter III. Once these parameters are separated it is easy to check the difference between their true values and the values at which they converge.

3. Fault Tolerant Control Allocation places no restriction on the magnitude of the desired control, which results in the non-existence of optimal solutions for a particular case. The design of some control scheme to handle such situations is needed. One of the ways to approach this problem is to tune gains in SAMI and restrict the commanded control. However to find a permanent solution to this problem reference trajectory can be changed accordingly to reach the final point or adaptive guidance can be used to generate the reference trajectory.

4. Fault Tolerant SAMI is well formulated to handle the proportional controls, but to handle the discrete jets, it needs an additional scheme of pulse width modulation. The scheme of pulse width modulation is not very easy to implement in

real-time, especially for a large number of control jets. An approach involving the extension of matrix theory could be considered to handle the discrete jets, as had been done for the proportional controls. Matrices can be constrained so that they can take only binary values to handle the discrete controls.

5. In the Fault Tolerant Control Allocation algorithm, a method to identify the failed jets is necessary. In this thesis it was assumed that the controller has the information about the failed jets *a priori*. H_∞ controller has been used successfully in the literature to identify failures. Same approach can be combined with this controller to identify failures.

6. One of the extensions can be to combine this work with the active on-line adaptive guidance where guidance can handle some of the uncertainties in the planet's atmosphere and can generate an online trajectory. Uncertainties in winds and density can be handled by putting appropriate constraints.

7. In this thesis over-actuated systems were considered for application of both the control algorithms. In future under-actuated systems can be considered and both the control algorithms can be applied to these systems. In under-actuated systems there are more states to be tracked than available controls. Fault tolerant control schemes can be applied to under-actuated systems by extending both the schemes presented in this thesis.

REFERENCES

[1] M. Bodson and J. Groszkiewicz, "Multivariable adaptive algorithms for reconfigurable flight control," *IEEE Transactions on Control Systems Technology*, vol. 5, no. 2, pp. 217–229, 1997.

[2] M. Bodson, "Evaluation of optimization methods for control allocation," *Journal of Guidance, Control, and Dynamics*, vol. 25, no. 4, pp. 703–711, July-August 2002.

[3] M. Tandale and J. Valasek, "Fault tolerant structured adaptive model inversion control," *Journal of Guidance, Control, and Dynamics*, vol. 29, no. 3, pp. 635–642, May-June 2006.

[4] H. Schaub, M.R. Akella, and J.L. Junkins, "Adaptive realization of linear closed-loop tracking dynamics in the presence of large system model errors," *The Journal of Astronautical Sciences*, vol. 48, no. 4, pp. 537–551, October-December 2000.

[5] K. Subbarao, A. Verma, and J.L. Junkins, "Structured adaptive model inversion applied to tracking spacecraft maneuvers," in *Proceedings of the AAS/AIAA Spaceflight Mechanics Meeting*, Clearwater, FL, 23-26 January 2000, number AAS-00-202.

[6] M. Tandale and J. Valasek, "Solutions for handling control position bounds in adaptive dynamic inversion controlled satellites," *Journal of Astronautical Sciences*, vol. 55, no. 2, pp. 171–194, April-June 2007.

[7] C. Restrepo and J. Valasek, "Structured adaptive model inversion controller for

Mars atmospheric flight," *Journal of Guidance, Control, and Dynamics*, vol. 31, no. 4, pp. 937–953, July-August 2008.

[8] K. Subbarao and J.L. Junkins, "Structured model reference adaptive control of a class of nonlinear systems," *Journal of Guidance, Control, and Dynamics*, vol. 26, no. 4, pp. 551–557, July-August 2003.

[9] B. Wie, *Space Vehicle Dynamics and Control*. 1801 Alexander Bell Drive, Reston, VA 20191 : American Institute of Aeronautics and Astronautics, Inc., 1998.

[10] P. A. Iannou and J. Sun, *Robust Adaptive Control*. Upper Saddle River, NJ : Prentice-Hall, Inc., 1996.

[11] W.C. Durham, "Constrained control allocation," *Journal of Guidance, Control, and Dynamics*, vol. 16, no. 4, pp. 717–725, July-August 1993.

[12] A.B. Page and M.L. Steinberg, "A closed-loop comparison of control allocation methods," in *Guidance, Navigation and Control Conference*, Denver, CO, 14-17 August 2000, number AIAA-2000-4538.

[13] R.H. Shertzer, D.J. Zimpfer, and P.D. Brown, "Control allocation for the next generation of entry vehicles," in *Guidance, Navigation and Control Conference*, Monterey, California, 5-8 August 2002, number AIAA-2002-4849.

[14] J.M. Buffington and D.F. Enns, "Flight control for mixed amplitude commands," *International Journal of Control*, vol. 68, no. 6, pp. 1209–1230, December 1997.

[15] D. Doman and A. Ngo, "Dynamic inversion based adaptive/reconfigurable control of the X-33 on ascent," *Journal of Guidance, Control, and Dynamics*, vol. 25, no. 2, pp. 275–284, March-April 2002.

[16] M.A. Bolender and D.B. Doman, "Non-linear control allocation using piecewise linear functions : A linear programming approach," *Journal of Guidance, Control, and Dynamics*, vol. 28, no. 3, pp. 558–562, May-June 2005.

[17] D. Doman, B. Gamble, and A. Ngo, "Control allocation of reaction control jets and aerodynamic surfaces for entry vehicles," in *AIAA Guidance, Navigation and Control Conference and Exhibit*, Hilton Head, SC, 20-23 August 2007, number AIAA-2007-6778.

[18] K. Subbarao, "Structured adaptive model inversion: Theory and applications to trajectory tracking for non-linear dynamical systems," Ph.D. dissertation, Aerospace Engineering Department, Texas A&M University, College Station, TX, 2001.

[19] G.V. Reklaitis, A. Ravindran, and K.M. Ragsdell, *Engineering Optimization-Methods and Applications*. New York : Wiley-Interscience Publication, 1983.

[20] G. Hadley, *Nonlinear and Dynamic Programming*. Reading, MA : Addison-Wesley Publishing Company, Inc., 1964.

[21] R.L. Graves and P. Wolfe, *Recent Adavnces in Mathematical Programming*. New York : McGraw-Hill Book Company, Inc., 1963.

[22] S.T. Glad, "On the gain margin of nonlinear and optimal regulators," *IEEE Transactions on Automatic Control*, vol. 29, no. 7, pp. 615–620, July 1984.

[23] D. Liberzon, *Switching in Systems and Control*. Boston, MA : Birkhauser, 1973.

[24] C.D. Persis, "On feedback stabilisation of nonlinear systems under quantization," in *Conference on Decision and Control and the European Control Conference*, Seville, Spain, 12-15 December 2005.

[25] D. Liberzon, "Quantization, time delays and nonlinear stabilization," *IEEE Transactions on Automatic Control*, vol. 51, no. 7, pp. 1190–1195, July 2006.

[26] E.D. Sontag, "Smooth stabilization implies coprime factorization," *IEEE Transactions on Automatic Control*, vol. 34, no. 4, pp. 435–443, April 1989.

APPENDIX A

TORQUE MATRIX

Torque matrix A is a 3×18 constant matrix composed of torques provided by each jet in three axes.

$$A = \begin{bmatrix} A_1 & A_2 & A_3 \end{bmatrix} \tag{A.1}$$

where

$$A_1 = \begin{bmatrix} -26.3200 & 0 & 26.3200 & 26.3200 & 0 & -26.3200 \\ 41.7200 & -41.7200 & -41.7200 & 41.7200 & -41.7200 & -41.7200 \\ -41.7200 & 41.7200 & -41.7200 & 41.7200 & -41.7200 & 41.7200 \end{bmatrix} \tag{A.2}$$

$$A_2 = \begin{bmatrix} -26.3200 & 0 & 26.3200 & 26.3200 & 0 & -26.3200 \\ 41.7200 & -41.7200 & -41.7200 & 41.7200 & -41.7200 & -41.7200 \\ -41.7200 & 41.7200 & -41.7200 & 41.7200 & -41.7200 & 41.7200 \end{bmatrix} \tag{A.3}$$

and

$$A_3 = \begin{bmatrix} -17.6000 & 0 & 17.6000 & 17.6000 & 0 & -17.6000 \\ 283.1000 & -283.1000 & -283.1000 & 283.1000 & -283.1000 & -283.1000 \\ -283.1000 & 283.1000 & -283.1000 & 283.1000 & -283.1000 & 283.1000 \end{bmatrix} \tag{A.4}$$

VITA

Monika Marwaha was born in Chandigarh, India. She earned the Bachelor of Engineering Degree (B.E) with distinction, from Punjab Engineering College, Chandigarh, India in aeronautical engineering in July 2004. Before joining Texas A&M University in Fall 2006 she worked as a Scientist in DRDL, Hyderabad, India. In August 2006, Monika Marwaha began her graduate studies under the advisement of Dr. John Valasek at Texas A&M. This thesis is the culmination of her graduate research and has been submitted in partial fulfillment of the requirements for a Master of Science degree in aerospace engineering. After completing her Master of Science degree she will continue her doctoral studies in aerospace engineering at Texas A&M University.

Contact Information: Dr. John Valasek, Department of Aerospace Engineering, Texas A&M University, College Station, TX 77843-3141.